Physics – Uspekhi **45** (8) 819 – 846 (2002)

REVIEWS OF TOPICAL PROBLEMS PACS numbers: 71.23.An, **71.55. – i**, 85.60.Gz

Mixed-valence impurities in lead telluride-based solid solutions

B A Volkov, L I Ryabova, D R Khokhlov

DOI: 10.1070/PU2002v045n08ABEH001146

Contents

Abstract. Experimental data on impurity states in narrow-gap lead telluride based semiconductors are summarized. Theoretical models describing the nontrivial properties of such states are presented. Applications to the design of highly sensitive far-infrared detectors are considered.

1. Introduction

Many and varied phenomena observed in doped IV – VI compounds not only amply demonstrate the potential of doped semiconductors in general but also reveal a number of properties that are unique to these compounds.

One of the distinguishing features of lead telluride is the combination of low effective masses with a high (up to 1000) static dielectric constant. The crystal lattice responds to charge exchange between impurities by becoming polarized and by screening possible charge fluctuations. The interaction of impurity centers with the lattice modifies the potential of an impurity atom and produces deep levels in the crystal's energy spectrum. The energy of these levels depends both on the type of the defect and on the way the defect interacts with its crystal environment.

It is known that in lead chalcogenides and their solid solutions, electrically active native point defects (vacancies and interstitial atoms) produce energy states lying either above the top of the conduction band (donor defects) or below the bottom of the valence band (acceptors) [1 – 4]. This leads to high charge carrier concentrations in undoped crystals because of the deviation of their composition from stoichiometry.

Furthermore, neither cooling nor a magnetic field have been observed to have the freeze-out effect on charge carriers [5]. It is this fact that to a large extent has limited the use of lead telluride and its solid solutions as optoelectronic detectors. As for doping with impurities, however, this 'disadvantage' of its crystal lattice becomes an advantage: one can not only use doping to change the carrier concentration but also observe effects that are due to the formation of a system of deep levels — both against the background of allowed energies and within the forbidden band.

The deep states result from the strongly localized potential of defects and cannot be described in a hydrogen-like approximation [6]. Because, further, these energy levels have no relation to the edges of the allowed bands genetically, the energy spectrum can be significantly modified by external factors such as the alloy composition, temperature, external pressure, and magnetic field. The first experimental evidence for the formation of deep levels and for Fermi level stabilization was found by doping lead chalcogenides with Group III elements In, Ga, and Tl [7].

B A Volkov P N Lebedev Physics Institute, Russian Academy of Sciences, Leninskiĭ prosp. 53, 117924 Moscow, Russian Federation
Tel. (7-095) 132 62 71. Fax (7-095) 135 85 83
E-mail: vlk@lpi.ru
L I Ryabova Chemistry Department,
M V Lomonosov Moscow State University,
Vorob'evy Gory, 119992 Moscow, Russian Federation
Tel. (7-095) 939 11 51. Fax (7-095) 932 88 76
E-mail: mila@mig.phys.msu.su
D R Khokhlov Physics Department,
M V Lomonosov Moscow State University,
Vorob'evy Gory, 119992 Moscow, Russian Federation
Tel. (7-095) 939 11 51. Fax (7-095) 932 88 76
E-mail: khokhlov@mig.phys.msu.su

Received 21 November 2001, revised 6 February 2002
Uspekhi Fizicheskikh Nauk **172** (8) 875 – 906 (2002)
Translated by E G Strel'chenko; edited by S N Gorin

Results highly unusual for narrow-band semiconductors were found. Solid solutions of lead telluride doped with indium and gallium were observed to relax very slowly when their electronic system was disturbed from equilibrium. A semi-insulating state and pressure- and magnetic-field-induced metal–insulator transitions were seen to occur. When lead telluride was doped with thallium, no long-term relaxation processes were observed. The Tl level located in the immediate neighborhood of the second valence subband caused a resonance scattering of holes and led to superconductivity [8, 9].

The list of impurity species leading to the stabilization of the Fermi level in lead telluride is continuously growing. At present, it is known also to include Cr, Yb, and Gd. Unfortunately, it is the trial-and-error efforts of experimenters rather than well-based theoretical predictions that provided these additions. This is due in large part to the fact that the stabilization phenomenon can only be proved to occur if the Fermi level is either in the forbidden band or lies against the background of the allowed energies not too far (100 meV or so) from the corresponding extrema. If an impurity level lies sufficiently high against the background of the allowed energies, then the stabilization of the Fermi level may be simply unachievable due to the limited solubility of the impurity.

The present review consists of four main parts. Part 2 discusses the experimental results on impurity states in lead telluride and its solutions. Basic information on the behavior of various impurities is presented, with special attention to the Fermi-level-stabilizing impurities. Of course, only well studied impurities of this kind are considered, and it is this group of impurities with which the remainder of the text is concerned. Part 3 presents the theoretical background for understanding the behavior of impurities in the compounds of interest. The applied aspects of the problem are discussed in Part 4.

The present review takes into account earlier review publications on the subject [7, 9–12], two of them [7, 9] in the *Physics–Uspekhi*. The 1998 review [9] focuses on the properties of thallium-doped lead chalcogenides. The most recent broad review of impurities for lead chalcogenides dates back seven years [12]. Since then, new experimental material has been gathered and new theoretical approaches have been developed. In this review we tried to study the problem in its development. However, to make the material accessible to a wide readership and to make the reader feel the specificity of the subject matter, we found it appropriate to briefly summarize the key aspects of the problem that have been discussed in detail in the previous publications.

2. Key experimental results on doped solid solutions

2.1 Charge carrier concentration as a function of the amount of a dopant. Fermi level stabilization

For the purposes of doping lead chalcogenides, various methodological approaches have been applied and many elements of the Periodic Table used. Nimtz and Schlicht [10] systematized the database on doping these materials and summarized it in a table titled 'Impurities and lead salts.' This database is supplemented by the data of more recent reviews [7–9, 11, 12].

One of the characteristic features of impurities in lead chalcogenides is that only very few of them may be uniquely classified as either donors (halogens) or acceptors (alkali metals Na and Li). Doping with these impurities increases the carrier concentration in proportion to the introduced amount of an impurity N_i up to 10^{20} cm^{-3} [7]. For most other dopants, to describe the dependence of the concentrations of free electrons n and holes p on N_i, additional factors should be taken into account, including the deviation from stoichiometry, the position of the dopant atom in the lattice, possible correlations between impurity atoms and native defects, and Fermi level stabilization.

It should be noted that impurities are far from always behaving in a manner consistent with theoretical expectations. According to Ref. [13], most rare-earth elements are donors in PbTe, but are trivalent when in compounds with tellurium. In monotellurides, Eu, Sm, Yb, and Tm are divalent and, so, were expected to be electrically neutral in PbTe, but this proved to be the case for Eu and Sm only. Thulium shows donor properties, increasing electron density in PbTe up to 10^{21} cm^{-3} [14]. Ytterbium forms an impurity band in the valence band of PbTe, which acts to stabilize the position of the Fermi level. The study of PbTe(Yb) is somewhat complicated by the fact that, unlike indium and gallium, introducing ytterbium markedly changes the width of the forbidden band E_g of the compound.

Transition metals also act as either donors (Cr, Co, Ni, Ti) or neutrals (Mn). When PbTe is doped with chromium, n increases to 1.3×10^{19} cm^{-3} and remains unchanged upon further increase of the concentration N_{Cr} up to the chromium solubility limit [15–19]. In PbSe(Cr), the saturation is observed at somewhat higher values of n (up to 1.8×10^{19} cm^{-3}). Importantly, isothermal annealing in lead or selenium vapors does not change the value of the stabilized electron density [20, 21]. In PbTe(Ti), the maximum electron density $n = 7\times10^{19}$ cm^{-3} was obtained at a concentration of $N_{Ti} = 0.3$ at. %. A further increase in titanium content (up to 0.5 at.%) had no effect on the value of n [22].

The system whose properties have been most widely studied and hence described in detail is PbTe and its solid solutions doped with In, Ga, and Tl. For each of these elements, the dependences n, $p(N_i)$ saturate, i.e., the position of the Fermi level is chemically stabilized. For PbTe(In) the saturation level corresponds to $n = 7\times10^{18}$ cm^{-3}; for PbTe(Tl), to $p = 10^{20}$ cm^{-3}. The charge carrier concentration remains unchanged on further doping with donors [iodine in PbTe(In), hyperstoichiometric Pb in PbTe(Tl)] and acceptors [Na in PbTe(Tl)] provided the concentration of the additional dopant does not exceed N_{In} and N_{Tl}. The chemical stabilization of the Fermi level has also been observed when introducing thallium into PbSe and PbS, with saturation hole concentrations of 10^{20} and 5×10^{19} cm^{-3}, respectively. In all cases, the hole density p was much lower than the thallium concentration N_{Tl} [7].

However, chemical stabilization is not always due to Fermi level stabilization by local and quasi-local levels. Nonlinear dependences n, $p(N_i)$ are observed quite often in lead chalcogenides. The data tabled in Nimtz and Schlicht's review [10] contain examples of impurities (Cu, Ag, Sb, Bi) that show either donor or acceptor properties depending on the deviation from the host-crystal stoichiometry. This may be due to the difference in electrical activity between dopant atoms occupying nonequivalent crystallographic positions. For example, the doping effect of Bi in stoichiometric

$Pb_{1-x}Bi_xTe$ is unstable, and the electron concentration is much lower than the introduced amount of Bi, N_{Bi}, the reason being the redistribution of Bi atoms between the chalcogen and metal sublattices [23]. Bismuth in the lead sublattice is in the donor state Bi^{3+}, and in the chalcogen sublattice Bi^{3-} is an acceptor. Such antisite Bi can be considered as a compensating impurity.

Research on doped lead salts over a wide range of deviations from stoichiometry was reviewed and analyzed in Refs [8, 9]. The experimental data were interpreted in terms of the self-compensation model. The term self-compensation implies that doping with donor or acceptor impurities stimulates the formation of native defects with the opposite electrical activity. Thus, the doping effect of an impurity can be suppressed to a large extent.

While self-compensated samples may have sufficiently low carrier concentrations, no local levels have been observed to form in the forbidden band. Self-compensation has been seen in PbTe, PbSe, and PbS on doping with Tl, Bi, I, Cl, Br, and In. The experimental data were approximated by assuming self-compensation by single vacancies, charged binary complexes, and neutral complexes. The theoretical calculations were generally in good agreement with experimental data. However, the properties of PbTe(In) and PbTe(Tl) cannot be explained in terms of self-compensation theory without invoking the formation of quasi-local levels in the allowed bands.

One further Group III element, gallium, displays a number of specific features when introduced into PbTe. By and large, gallium may be considered as a donor. According to various authors [24–28], there are at least two saturation regions in the n, $p(N_{Ga})$ dependences. One occurs immediately after the conduction reverses from the p to the n type and corresponds to nearly intrinsic electron density ($n < 10^{13}$ cm^{-3} at a temperature $T = 77$ K) and to high sample resistances. The concentrations N_{Ga} corresponding to this saturation region depend on the preparation method and range from 10^{19} to 10^{20} cm^{-3} according to various studies [24–26, 28].

The second saturation region is observed at higher gallium concentrations, $N_{Ga} > 10^{20}$ cm^{-3}, and corresponds to the electron concentration $n = 2 \times 10^{18}$ cm^{-3} [26]. Sintered samples reveal electron concentration stabilization at a level of $n = 6 \times 10^{19}$ cm^{-3} for a Ga concentration $N_{Ga} = 5 \times 10^{20}$ cm^{-3} [28]. There is general agreement, however, that in n-PbTe(Ga) the inequality $n \ll N_{Ga}$ is always fulfilled under the electron-concentration stabilization conditions.

From an application viewpoint, that saturation region in the p, $n(N_{Ga})$ curve that corresponds to the sample's semi-insulating state can be considered the most important. It is no wonder, therefore, that this region has been the main subject of experimental research. The distinguishing feature of this region as compared to In- or Cr-doped PbTe is the narrow range of concentrations N_{Ga}. This has given rise to the fully justifiable suspicion that the semi-insulating state of PbTe(Ga) might be due to the high degree of compensation in the sample, with no relation to the Fermi-level stabilization in the forbidden band.

The argument in favor of the Fermi-level stabilization hypothesis has been that, irrespective of the synthesis method, the semi-insulating samples have highly reproducible electrical and physical parameters. For all the crystals studied, an activation region was observed on the temperature dependences of the resistivity ρ and the Hall coefficient R_H. The energy of activation of an electron from a donor level as calculated by the formula $\rho \propto \exp(E_a/kT)$ was $E_a = 70$ meV [29–31].

Direct experimental evidence for Fermi-level stabilization came from the studies of the effect of fast-electron irradiation on the galvanomagnetic characteristics of PbTe(Ga) [32]. According to Ref. [33], radiation defects in lead chalcogenides act as donors. Thus, in irradiation experiments the level of compensation in the host sample could be varied smoothly, without significantly heating the material. This last circumstance is of key importance, because annealing of the samples leads to irreversible changes in their electrical and physical parameters [34]. Heating a semi-insulating sample of PbTe(Ga) from room temperature to 250 °C, maintaining this temperature for a few minutes, and then cooling the sample back to room temperature increased the free-electron concentration to as high values as $n = 10^{18}$ cm^{-3}.

The samples chosen for fast-electron irradiation experiments were of two types, p-PbTe(Ga), with an insufficient gallium concentration to reverse the conduction type, and semi-insulating n-PbTe(Ga) samples. Irradiating p samples led to conduction reversal and subsequently to a semi-insulating state, which remained stable as the radiation dose Φ was further increased. The temperature dependences of the resistivity ρ and Hall coefficient R_H in p-PbTe(Ga) were obtained by gradually increasing the radiation dose Φ and are shown in Fig. 1. The parameters of n-PbTe(Ga) samples remain stable up to a dose $\Phi = 2 \times 10^{17}$ cm^{-2}.

Two of the most attractive properties of doped semiconductors with a stabilized Fermi level are uniform electrical and physical parameters and the high mobility μ of charge carriers even at large carrier concentrations n and p. Doping PbTe samples with indium and PbTe and PbSe samples with chromium up to $N_i = 0.5$ at. % did not lower μ. In the best-quality samples, the value of μ reached 10^5 cm^2 V^{-1} s^{-1} at the temperature of liquid helium [19, 20, 35, 36].

The magnetoresistance of PbTe(In) samples saturates in strong magnetic fields, consistent with the theory of homogeneous semiconductors [37]. PbTe(In) and PbTe(Cr) samples show clear Shubnikov–de Haas oscillations (Fig. 2). In PbTe(Cr) with an electron concentration above 10^{19} cm^{-3}, over 100 oscillation extrema with clear spin splitting can be seen at $T = 2.1$ K in magnetic fields of up to 6 T. From an analysis of oscillation dependences obtained at various temperatures, the contribution of the exchange interaction with chromium ions to the g factor of the conduction electrons [15–17] was estimated.

The properties of thallium-doped lead telluride are determined to a large extent by the fact that the valence subband of heavy holes is close to a quasi-local thallium level located at 0.15–0.25 eV below the top of the light-hole valence band. The broadening of the thallium level is also an important factor [9]. For PbTe(Tl) samples corresponding to the saturation region on the $p(N_{Tl})$ dependences, the resonance scattering of holes is observed.

The scattering cross section depends on the width of the impurity band and the position of the Fermi level within it [38]. The most intriguing property of PbTe(Tl) samples is superconductivity [39]. The superconducting transition temperature depends on the ratio between the concentrations of thallium and an additional dopant (Li, Na) in samples with a fixed hole concentration [40]. The maximum transition temperature is 2.2 K. This can be considered quite a large value for a semiconductor.

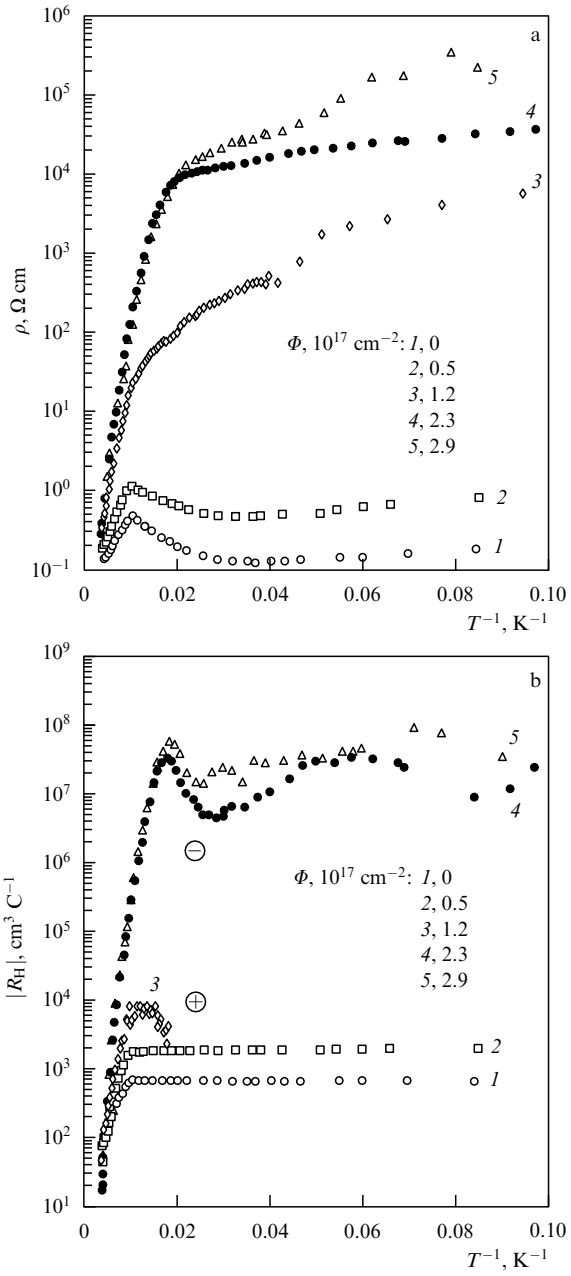

Figure 1. Temperature variation of (a) the resistivity ρ and (b) the Hall coefficient R_H in a *p*-PbTe(Ga) sample for various fast-electron irradiation doses Φ [32].

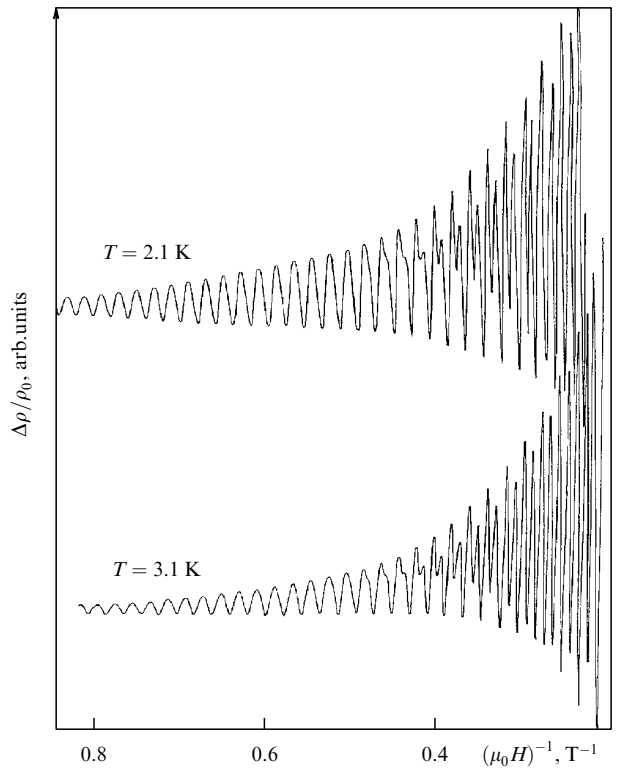

Figure 2. Magnetoresistance oscillations in a PbTe(Cr) sample with $n = 1.2 \times 10^{19}$ cm^{-3} at $H \| \langle 100 \rangle$ [17].

The existence of a thallium impurity level (band) is supported by experiments on optical absorption, tunneling spectroscopy, low-temperature heat capacity, magnetic susceptibility, superconductivity, and other transport properties, and also self-compensation. The properties of thallium-doped lead chalcogenides have been systematized very thoroughly in a number of review papers [9, 38], this making our task here much easier. Without going into details, we will only present characteristic energy levels of thallium as an impurity in the compounds mentioned above. At temperatures $T \to 0$, the impurity level in PbTe(Tl) lies 0.22 eV below the top of the valence band [41, 42], whereas for PbSe(Tl) and PbS(Tl) these energies are 0.26 and 0.15 eV, respectively, at $T = 77$ K [43, 44]. Quasi-local states have also been observed in the valence bands of lead chalcogenides doped with isoelectronic impurities Sn and Ge [45, 46].

The most detailed experimental study of local and quasi-local states subject to external influences have been made on lead telluride and a number of its solid solutions. Compared to other lead chalcogenides, the stabilized Fermi level in these compounds is closest to the edges of the allowed bands. For example, in PbTe(In) the impurity level is 0.07 eV above the conduction-band bottom, in PbSe(In) it is 0.3 eV above the conduction-band bottom, and in PbS(In) even higher [7]. Thus, the study of the two last compounds is complicated by high concentrations of free electrons.

2.2 Externally induced energy-spectrum rearrangement in doped lead telluride and its solid solutions. Experimental evidence for Fermi-level stabilization

2.2.1 Temperature. The first experimental evidence for Fermi-level stabilization in PbTe(In) was obtained by measuring the temperature dependence of the Hall coefficient R_H. Data for PbTe(In) [37] and those obtained somewhat later for PbTe(Cr) [36, 47] differed qualitatively from data on lead telluride samples doped with halogens or native donor defects and having similar electron concentrations. In the latter case, the electron concentration remains constant up to about room temperature. In PbTe(In) and PbTe(Cr), a significant nonmonotonic change in R_H with temperature was observed. This effect was explained in terms of the electron-concentration change due to the stabilized Fermi level shifting relative to the conduction-band edge with changing temperature. For both compounds, the coefficient dE_i/dT was found to be nearly the same, $(3 \pm 1) \times 10^{-4}$ eV K^{-1}.

The $R_H(T)$ dependence for *p*-PbTe(Tl) is much harder to interpret, because heavy holes of the second valence subband

contribute substantially to conduction. If the density of states in the impurity subband is low, an increase in temperature induces hole transitions from the light valence band to the impurity band. For higher densities of states, the reverse process occurs. The result is a significant difference in $R_H(T)$ dependences for samples with different densities of states in the impurity band [7].

In PbTe(Yb) crystals, an impurity level was also found to shift toward the top of the valence band as the temperature was increased [48].

2.2.2 Solid-solution composition. At present, a sufficiently large number of solid solutions on the basis of doped PbTe are known to exhibit Fermi-level stabilization. These compounds and their most characteristic properties are listed in the table. Of course, these materials have been studied to varying degrees of detail, and not for all of them can the stabilization effect be claimed confidently. We consider it is appropriate, however, to present all the available data and to compare them with those for the most thoroughly studied solid solutions — such as $Pb_{1-x}Sn_xTe(In)$, for example.

Table. Basic properties of solid solutions on the basis of doped lead telluride.

Compound	Properties
PbTe(In)	$n = 6 \times 10^{18}$ cm^{-3}, $E_F - E_c = 70$ meV, $T_c = 20$ K
PbTe(Ga)	$E_c - E_F = 65 - 70$ meV, $T_c = 80$ K
PbTe(Cr)	$n = 1.3 \times 10^{19}$ cm^{-3}, $E_F - E_c = 100$ meV, SMSC
PbSe(Cr)	$n = 1.8 \times 10^{19}$ cm^{-3}, $E_F - E_c = 125$ meV, SMSC
PbTe(Tl)	$p > 10^{19}$ cm^{-3}, Superconductivity at $T < 3$ K
PbTe(Yb)	$E_F \approx E_v$
$Pb_{1-x}Sn_xTe(In)$	Semi-insulating state at $0.22 < x < 0.28$, $T_c = 20$ K
$Pb_{1-x}Sn_xTe(Ga)$	$n-p$ conversion under pressure
$Pb_{1-x}Mn_xTe(In)$	Semi-insulating state at $x > 0.05$, $T_c = 20$ K
$Pb_{1-x}Mn_xTe(Ga)$	Semi-insulating state at $T_c = 80$ K
$Pb_{1-x}Ge_xTe(In)$	Semi-insulating state at $x > 0.08$, $T_c = 80$ K
$Pb_{1-x}Ge_xTe(Ga)$	Semi-insulating state at $T_c = 80$ K
$Pb_{1-x-y}Mn_xYb_yTe$ $0.0201 < x < 0.0239$ $0.054 < y < 0.0103$	p conduction, semi-insulating state, increase in $E_v - E_F$ with increasing x and y
$Pb_{1-x}Ge_xTe(Yb)$	Metal–insulator transition at $x = 0.01$
$Pb_{1-x-y}Sn_yGd_xTe$ $x = 0.04$	$n-p$ conversion with increasing y

Note: SMSC, semimagnetic semiconductor; T_c, persistent photoconductivity onset temperature; the values of n, p, and E_F are given for $T = 4.2$ K.

It should be noted here that the $n, p(N_i)$ dependences have only been investigated for binary compounds. For ternary doped compounds, the problem of confidently fixing the composition for various dopant concentrations not only complicated experiments but indeed put their very advisability in doubt. In addition, the absence of extended saturation regions on $n, p(N_i)$ dependences does not exclude the Fermi-level stabilization effect, which is true, in particular, for PbTe(Ga). It is for this reason that the evidence for the stabilization effect in solid solutions has been looked for through the use of external influences — those that permitted the Fermi level to be shifted relative to the edges of the allowed bands.

All solid solutions doped with In or Ga are characterized by a negative value of the coefficient $\partial(E_F - E_c)/\partial x$ irrespective of the sign of the coefficient $\partial E_g/\partial T$ that characterizes the change of the gap with temperature. In In-doped solid solutions $Pb_{1-x}Sn_xTe(In)$ [49, 50], $Pb_{1-x}Mn_xTe(In)$ [51], and $Pb_{1-x}Ge_xTe(In)$ [52, 53], this gives rise to metal–insulator transitions, in which the Fermi level crosses the conduction-band edge at a certain value of x. The rearrangement of the energy spectrum with composition change in $Pb_{1-x}Sn_xTe(In)$ and $Pb_{1-x}Mn_xTe(In)$ is illustrated by diagrams in Fig. 3a.

For the $Pb_{1-x}Sn_xTe(In)$ alloys, the Fermi level is found to be stabilized in the forbidden band in the composition range $0.22 < x < 0.28$ [49]. According to Ref. [50], this range is somewhat different. For the alloys in the above range, the concentration of free charge carriers is found to be below 10^{10} cm^{-3} at liquid-helium temperatures. At $x = 0.26$, the Fermi level crosses the middle of the forbidden band and the $n-p$ conduction inversion occurs.

For $Pb_{1-x}Mn_xTe(In)$, the metal–insulator transition is observed for $x = 0.05$. It should be noted that the solid

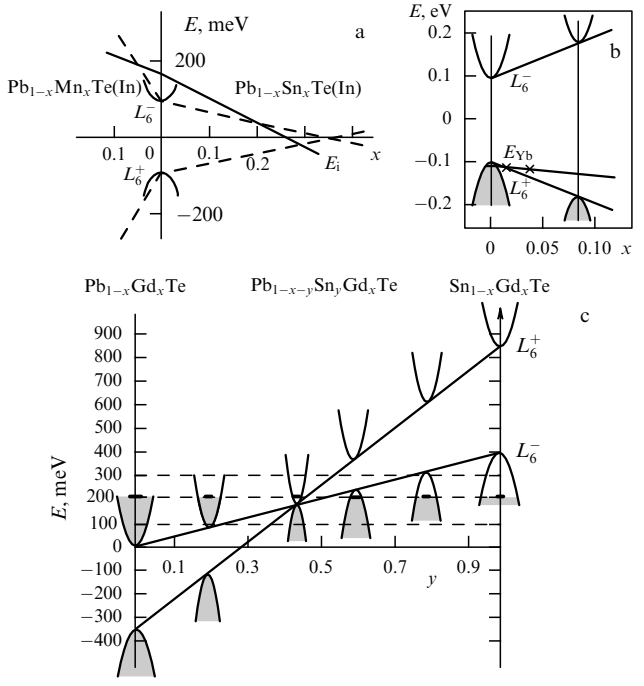

Figure 3. Schematic diagram for energy-spectrum rearrangement with the variation in alloy composition for (a) $Pb_{1-x}Sn_xTe(In)$ and $Pb_{1-x}Mn_xTe(In)$ for $T \to 0$ [12]; (b) $Pb_{1-x}Ge_xTe(Yb)$ for $T = 4.2$ K [61]; and (c) $Pb_{1-x-y}Sn_xGd_yTe$ [62].

solutions $Pb_{1-x}Mn_xTe$ exist at $x \leqslant 0.20$, whereas In-doped alloys have been studied only for $x < 0.1$ [27]. In $Pb_{1-x}Ge_xTe$(In), the metal–insulator transition occurs at $x = 0.08$ [52, 53]. Doping with indium leads to a marked decrease in the ferroelectric transition temperature in this alloy.

Doping $Pb_{1-x}Mn_xTe$(Ga) and $Pb_{1-x}Ge_xTe$(Ga) with gallium shifts the Fermi level down in energy, away from the conduction-band bottom. However, the inversion of the conduction type has not been observed in the composition range studied [54, 55].

Relatively recently it has been established that in PbTe(Yb) the impurity level lies in the valence band, close to its edge [48, 56 – 59]. A tendency of the Fermi level to shift into the forbidden band in the $Pb_{1-x}Ge_xTe$(Yb) alloys was observed in Refs [56, 59], while Refs [60, 61] report activated impurity conduction at $x \geqslant 0.01$ and the growth of the activation energy at a rate $\partial(\Delta E_{Yb})/\partial x = 7$ meV (at. %)$^{-1}$ (Fig. 3b).

Studies of how the energy spectrum rearranges itself with changes in the composition of $Pb_{1-x}Sn_xTe$(Gd) alloys have suggested the possibility that the pinning of the Fermi level may occur in this solid solution as well [62]. Estimates put the impurity energy level of gadolinium in PbTe high in the conduction band ($E_F - E_c = 200$ meV), and in SnTe, deep in the valence band. Electrical conductivity, Hall effect, and magnetic susceptibility measurements on the solid solutions $Pb_{1-x-y}Sn_xGd_yTe$ have shown that crystals with $y < 0.6$ have only electron conduction and those with $y > 0.6$, only hole conduction. The authors of Ref. [62] explained the experimental results by the fact that the Gd level, stabilizing the position of the Fermi level, shifts as the content of Sn changes (Fig. 3c). These conclusions can only be considered preliminary, however, because a detailed study of these complex solid solutions has not been conducted so far — certainly not in the composition range near the inversion point.

A shift of the Fermi level to the conduction-band edge (i.e., a decrease in $E_F - E_c$) in the solid solutions $Pb_{1-x}Sn_xTe$(Cr) was observed in Ref. [63] for compositions with $x < 0.2$.

2.2.3 Hydrostatic compression. Hydrostatic pressure P is yet another factor affecting the relative positions of the stabilized Fermi level and the edges of the allowed bands. In lead telluride, as well as in PbSe and PbS, the extrema of the L_6^+ and L_6^- bands approach each other, and at a certain pressure $P = P_i$ a gapless state is produced. The gapless state corresponds to the point where a transition to the inverse region of the spectrum occurs. In the region of the direct spectrum ($P < P_i$), the term L_6^- corresponds to the conduction band, and the term L_6^+, to the valence band. For the inverse spectrum ($P > P_i$), the terms change places. Thus, lead telluride and its solid solutions have a negative coefficient $\partial E_g/\partial T$ in the direct spectrum region and a positive $\partial E_g/\partial T$ in the inverse region.

In the presence of the stabilization effect, the Fermi level in compressed $Pb_{1-x}Sn_xTe$(In) alloys shifted very little relative to the middle of the forbidden band, and in solid solutions with $0.22 < x < 0.28$, a sequence of metal–insulator–metal transitions were observed [64]. In PbTe(Cr), pressure also caused a significant change in electron concentration, with the Fermi level remaining practically stabilized relative to the middle of the gap [36].

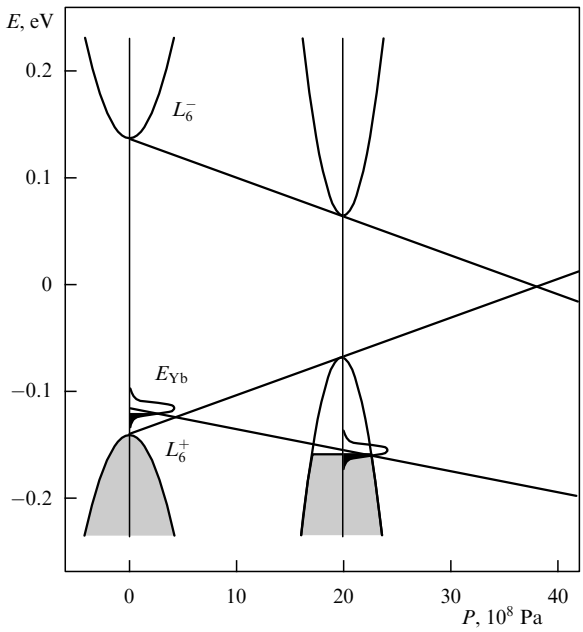

Figure 4. Energy spectrum of $Pb_{1-x}Ge_xTe$(Yb) ($x = 0.038$) versus pressure for $T = 4.2$ K [61].

The study of pressure-induced spectrum rearrangements in solid solutions $Pb_{1-x}Ge_xTe$(Yb) for $x \leqslant 0.04$ showed that the Yb level, lying in the energy gap under normal pressure, shifts to the top of the valence band at a rate $\partial(\Delta E_{Yb})/\partial P = 5 \times 10^{-8}$ meV Pa^{-1} (Fig. 4). Pressure induces an insulator–metal transition. The increase in the hole concentration is explained as resulting from the transition of electrons from the valence band to an impurity level. Analysis of the experimental and calculated $E_F(P)$ dependences reveals that the ytterbium level is broadened and has a width of about 7 meV and a sufficiently high density of states, $N_{Yb} \sim 10^{20}$ cm^{-3} [60, 61].

Applying pressure to semi-insulating n-PbTe(Ga) samples lowered the activation energy for impurity conduction and $n-p$ conversion at $P \sim 10^9$ Pa [35]. An interesting result was obtained in the study of the solid solutions $Pb_{1-x}Sn_xTe$(Ga) under pressure [65]. In n-type alloys, applying pressure caused the Fermi level to make a sharp jump from the conduction to the valence band. The nonmonotonic behavior of $E_F(P)$ observed in the experiments was explained in terms of the change in the charged state of a gallium impurity in the crystal lattice. The electrically active donor center of gallium became neutral in the process. The lack of Fermi-level stabilization in the samples studied was presumably due to the excessive dopant content.

These data indicate that charge states of gallium are unstable toward possible lattice stresses and can be affected by small atomic displacements due to the unit-cell deformation. This picture was confirmed in the study of the solid solutions $Pb_{1-x}Ge_xTe$(Ga) [55]. A sharp drop in the resistivity was observed at a temperature 80 K below the ferroelectric transition temperature for all the alloy compositions studied. However, whereas in the case of $Pb_{1-x}Sn_xTe$(Ga) the absence of the Fermi level stabilization was only a guess, for $Pb_{1-x}Ge_xTe$(Ga) samples this fact was confirmed by irradiation experiments [66]. Furthermore, the energy spectrum of $Pb_{1-x}Ge_xTe$(Ga) at $0.04 \leqslant x \leqslant 0.08$ showed an additional impurity level in the forbidden band [66]. Extrapolation to

lower values of x indicated that in PbTe(Ga) this level should lie in the conduction band.

The totality of the experimental data show that the energy spectrum of PbTe(Ga) and its solid solutions is sufficiently complex and that the presence of a dopant is not tantamount to the formation of a single Fermi-level-stabilizing impurity level.

2.2.4 Magnetic field. The magnetic field, as an external parameter, has a characteristic feature which distinguishes it from such influences as pressure P or the variation of the alloy composition x. In compression experiments, P was varied at room temperature. The subsequent measurements of alloy parameters at low temperatures corresponded to a certain stationary state with x and P fixed.

A magnetic field is applied directly at low temperatures. Consequently, the kinetic factor, due to magnetic-field-induced nonequilibrium processes, becomes important. When the magnetic field strength H exceeds the ultraquantum limit H_{uql}, the density of states below the Fermi level in the 0^- Landau subband starts to increase. At low temperatures charge carriers may take a long time to overflow to the 0^- band, and in the systems studied a nonequilibrium state is realized. Accordingly, when the magnetic field is turned off, the quasi-Fermi level corresponding to the carrier concentration at $H > H_{\text{uql}}$ is above the equilibrium-state stabilized Fermi level. Note that the localization of nonequilibrium charge carriers also may be a long-term process.

The overflow of charge carriers in a magnetic field is illustrated by diagrams in Fig. 5 [67]. The spectrum of the $Pb_{1-x}Sn_xTe(In)$ alloy in the metallic state ($E_F > E_c$) without a magnetic field is shown in Fig. 5a. Figure 5b shows the change of the energy spectrum in a magnetic field $H > H_{\text{uql}}$ for the case in which spin splitting is less that the orbital splitting (the effective g factor is less than 2). In this case, only the states in the 0^- Landau subband are below the Fermi level (the parabola corresponds to the continuous spectrum in the direction k_z).

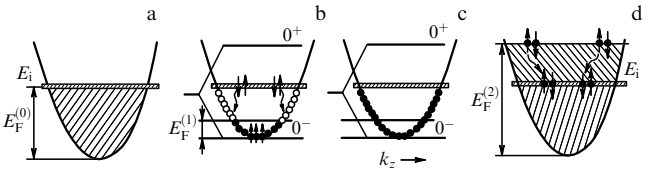

Figure 5. Cycle of the formation of a nonequilibrium state in a magnetic field (see text). Solid and open circles denote the filled and free states, respectively [67]).

The equilibrium situation for $H > H_{\text{uql}}$ is illustrated in Fig. 5c. Immediately after the magnetic field is turned off, the quasi-Fermi level is above the stabilized Fermi level, and a nonequilibrium situation is realized again (Fig. 5d). Long-term relaxation processes in a magnetic field are a separate problem, to which we address ourselves in Section 4. In the present section, only the equilibrium situation is considered.

Solid solutions $Pb_{1-x}Sn_xTe(In)$ proved to be all but ideal for investigating the Fermi-level-stabilization effect and how the energy spectrum rearranges itself in ultraquantum magnetic fields. By varying the composition x and applying the pressure P, the arrangement of the Fermi level and allowed-band edges can be optimized with respect to the experimentally achievable values of H_{uql}. Furthermore, one can choose the n ($x < 0.22$) or p ($x > 0.28$) conduction type as well as the direct ($P < P_i$) or inverse ($P > P_i$) region of the spectrum [68]. In all the experiments discussed below, the magnetic field vector is taken along the crystallographic direction $\langle 100 \rangle$, for which four isoenergetic ellipsoids of the Fermi surface are positioned equivalently with respect to the vector **H**.

Figure 6 presents the field dependences of the Hall voltage $U_H(H)$ for a $Pb_{1-x}Sn_xTe(In)$ sample of p type ($x = 0.30$) measured at varying rates dH/dt. On turning the magnetic field on and off, curves *1–3* exhibit hysteresis, due to slow relaxation processes. The $U_H(H)$ dependences can be considered stationary only at $T > 15$ K. The fact that nonlinear regions in the curve appear precisely in the range $H > H_{\text{uql}}$ (curve *3* is close to being stationary) is illustrated by Shubnikov–de Haas oscillations (curve *4*). The ultraquantum-limit field can be estimated from the position of the last oscillation extremum on the magnetoresistivity dependences $\Delta\rho(H)/\rho_0$.

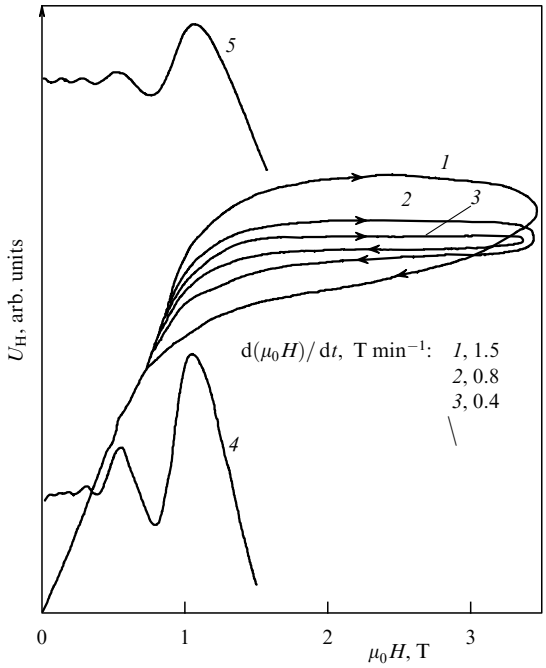

Figure 6. Magnetic field dependences of the Hall voltages $U_H(H)$ (curves *1–3*); magnetoresistance $\Delta\rho(H)/\rho_0$ (curve *4*); and the normalized Hall voltage $\Delta U_H(H)/U_0$ (curve *5*) for the $Pb_{0.70}Sn_{0.30}Te(In)$ sample. Curves *2–3* differ in the recording rate dH/dt. The monotonic regions of $\rho(H)$ and $U_H(H)$ are compensated, $P = 9.2 \times 10^8$ Pa, $T = 4.2$ K [68].

The stationary dependences $U_H(H)$ for $H > H_{\text{uql}}$ differ qualitatively in the regions of direct and inverse spectra. For $P < P_i$, the function $U_H(H)$ is weakly increasing, and for $P > P_i$, weakly decreasing. Near the gapless state, the function $U_H(H)$ remains virtually constant. This feature is observed both in n- and p-type alloys.

The way in which the charge carrier concentration in the ultraquantum limit of magnetic fields, $n_{\text{uql}}(H)$, depends on the field under conditions of stabilized Fermi level position was analyzed in detail in Refs [67–69]. The linear increase in $n_{\text{uql}}(H)$ in a magnetic field is found to be realized only for the g-factor value $g = 2$ (gapless state). The stationary value

of the Hall voltage is then given by the relation

$$U_{\rm H}(H) = \text{const}\,\frac{H}{n_{\rm uql}(H)} \qquad (2.1)$$

and $U_{\rm H}$ does not change at $H > H_{\rm uql}$.

The deviations of the experimental dependences $U_{\rm H}(H)$ from Eqn (2.1) that are observed in the direct and inverse spectra are due to the deviation of the g factor from the value $g = 2$. The analysis of the curves yielded g factors for $Pb_{1-x}Sn_xTe$ as functions of the gap width. Calculated in this way, the values of g factors correlate well with measurements of impurity activation energies on insulating $Pb_{1-x}Sn_xTe$(In) alloys in a magnetic field.

While experiments in a magnetic field have convincingly demonstrated Fermi-level stabilization in $Pb_{1-x}Sn_xTe$(In), this is thus far the only system to have exhibited the effects discussed. To our knowledge, with the only exception of solid solutions based on doped lead chalcogenides, Fermi-level stabilization against the background of the band continuum has been observed only in the family of HgSe(Fe)-based materials [19, 70]. In these materials, as well as in PbTe(Cr) and PbTe(Tl), the Fermi energies are sufficiently high, so that the ultraquantum-limit field lies in the region of superhigh magnetic fields.

One further point to remember is that band-edge shifts in lead chalcogenides are very small (for PbTe, $\partial E_{\rm g}/\partial(\mu_0 H) = 1$ meV T^{-1}) in comparison with the Fermi energy (of order 100 meV). Effects in a magnetic field up to 6 T are quite pronounced if the Fermi level is ± 15 meV from the edge of the nearest band. Thus, even a slight modulation of the band edge will affect the results. One cannot rule out the possibility that it is precisely this fact that did not permit the study of the magnetic-field-induced spectrum rearrangement in $Pb_{1-x}Mn_xTe$(In) solid solutions, materials in which the coefficient $\partial E_{\rm g}/\partial x$ is much higher [40 meV (mol. % MnTe)$^{-1}$] than in $Pb_{1-x}Sn_xTe$(In) [5.4 meV (mol. % SnTe)$^{-1}$] and in which even slight fluctuations in the composition x may considerably modify the band-edge modulation.

The broadening of impurity levels, which is quite significant in PbTe(Tl) and solid solutions on the basis of Yb-doped lead telluride, is yet another factor complicating the study of the energy spectrum in a magnetic field. In view of the above considerations, it is clear how uniquely suitable the $Pb_{1-x}Sn_xTe$(In) alloys are for the study of energy-spectrum rearrangement in a magnetic field.

Still, in alloys where an impurity level is broadened and so is in fact an impurity band rather than a level, interesting effects of a qualitatively different nature are observed. In semimagnetic solid solutions $Pb_{1-x-y}Mn_xYb_yTe$ ($0.0201 < x < 0.0239$, $0.0054 < y < 0.0103$), a giant negative magnetoresistance was discovered at low ($T \leqslant 15$ K) temperatures (Fig. 7) [71]. To explain this effect even at a qualitative level proved to be quite a challenge. Since neither indium- or gallium-doped $Pb_{1-x}Mn_xTe$ alloys nor ytterbium-doped $Pb_{1-x}Ge_xTe$ alloys exhibited giant negative magnetoresistance, it was assumed [71] that the superposition of two factors, namely, the presence of a magnetic component in the solid solutions and a sufficiently wide impurity band, could be the answer.

In fact, unlike the indium case, ytterbium-based impurity levels are not strongly localized, and the nature of transport in the system under study depends very much on the density of states in the impurity band. At high temperatures the

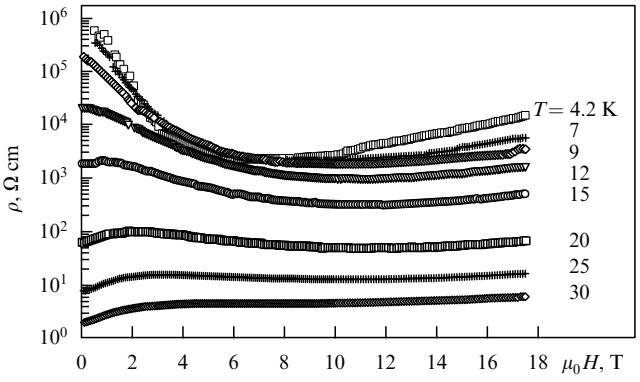

Figure 7. Magnetoresistivity of the $Pb_{1-x-y}Mn_xYb_yTe$ ($x = 0.0239$, $y = 0.0054$) sample for various temperatures [71].

conductivity of the $Pb_{1-x-y}Mn_xYb_yTe$ alloys is of an activation nature, due to the excitation of levels from an impurity level to the valence band. At low temperatures, activation to the mobility threshold and percolation processes determine the conductivity.

In lead telluride-based alloys, the exchange interaction of the d electrons of manganese with free carriers is especially important for materials with p-type conduction, because the value of the exchange integral for holes is much larger than that for electrons. Since the ytterbium level is rather close to the valence band ($E_{\rm a} \leqslant 32$ meV), the hybridization of the wave functions of the impurity and band states cannot be ruled out.

Thus, the d states of Mn may also influence states in the impurity band. In a magnetic field, a change in the density-of-states profile and, as a consequence, a change in the Fermi-level position with respect to the percolation threshold, can be observed. Also, the influence of magnetic-field-induced spin polarization cannot be excluded. Clearly, the arguments given in Ref. [71] are quite general, and further theoretical work is needed.

2.3 Long-term relaxation processes

In the preceding section, our concern was with the stationary state of doped lead chalcogenide-based alloys with a stabilized Fermi level. The question of precisely how this state was reached was not discussed. However, nonequilibrium processes occurring in the compounds of interest here are unusual in many respects and in some cases unique. In this section, we consider nonequilibrium phenomena that involve long-term relaxation processes. 'Long-term' in this context should be understood in a literal sense, i.e., the time it takes the system to reach equilibrium is not compared with the lifetime of electronic excited states but rather is measured in hours or tens of hours or even may be indefinitely long.

Such processes are observed, in particular, in a number of indium- or gallium-doped lead telluride-based solid solutions at low temperatures [12]. In PbTe(Tl) and PbTe(Cr), no long-term relaxation processes have been observed experimentally. This does not mean, however, that they do not occur there: simply, at carrier concentrations in excess of 10^{19} cm^{-3}, a nonequilibrium state is quite difficult to realize and study. Relatively recently, persistent photoconductivity has also been seen in $Pb_{1-x}Ge_xTe$(Yb) solid solutions [72].

It should be noted that persistent photoconductivity was discovered in semiconductors over 50 years ago and has since

been studied in detail. The first reports on this phenomenon came from research on inhomogeneous materials with an energy-band modulation. Recombination barriers, either due to the fluctuating space charge of defects or to the nonuniform distribution of solid-solution components, resulted in the spatial separation of nonequilibrium carriers and led to the freeze-out of the nonequilibrium state for an indefinitely long time. This process was analyzed in detail in Sheĭkman and Shik's review [73].

Persistent photoconductivity has been repeatedly observed in quantum-well structures. Both positive and negative photoconduction responses have been reported [74]. The mechanism responsible for this effect is essentially identical to that described in Ref. [73]. The only difference is basically that in inhomogeneous semiconductors barriers appear in a spontaneous and random fashion, whereas in quantum-well structures they are planned beforehand.

Persistent photoconductivity in semiconductors containing DX centers is qualitatively different. A recombination barrier in this case is due to correlation effects in the impurity–crystal lattice system. According to current views, a change in the charge state of an impurity center involves the rearrangement of the nearest crystal-lattice environment. This process is illustrated schematically by diagrams representing the dependence of the energy of a center on a configuration coordinate [75].

Persistent photoconductivity in doped lead telluride-based solid solutions has much in common with that in systems with DX centers. However, there are also aspects that make these solid solutions qualitatively different from classical semiconductors, including those with DX centers. An important point to note is that systems with DX centers are characterized by a negative correlation energy, and impurity levels in them form within the forbidden band. Therefore, nonequilibrium processes with long-term kinetics correspond to the nondegenerate statistics of charge carriers.

Although PbTe(In) and some of its solid solutions have their Fermi level stabilized in the conduction band, they have been found to exhibit long-term relaxation processes — induced not only by illumination but also by magnetic fields $H > H_{uql}$. The slow reduction of the Fermi surface in $Pb_{1-x}Sn_xTe(In)$ alloys and the associated change in the period of Shubnikov–de Haas oscillations are two features that thus far can be considered unique to these semiconducting materials.

We next turn to consider experimental data in more detail, starting our discussion with nonequilibrium processes in a magnetic field. What makes the magnetic field advantageous as an external influence for creating nonequilibrium processes is that the excitation it produces is uniform throughout a bulk sample. IR illumination far from always creates a state which is equilibrium throughout the entire volume. However, there are also factors that complicate the interpretation of kinetic processes in a magnetic field, namely, spin polarization and possible tunneling. The study of nonequilibrium situations created by various external influences provides the most complete and reliable information about impurity states and the contribution they make to long-term relaxation processes.

2.3.1 Long-term relaxation processes in a magnetic field. Let us return to the diagram for the *n*-type $Pb_{1-x}Sn_xTe(In)$ alloys in the metallic state shown in Fig. 5. The overflow of electrons in the presence of a magnetic field, which is denoted by arrows in the figure, is a long-term process. This is clearly seen from the Hall-effect data (see Fig. 6). The analysis of the $U_H(t)$ dependences after the turn-on (Fig. 5b, electrons flow from the stabilized Fermi level to the 0^- Landau subband) and turn-off (Fig. 5d, electrons flow from the quasi-Fermi level to the conduction band) of fixed magnetic field showed that relaxation to equilibrium cannot be described by exponential kinetics with constant characteristic times τ_1 and τ_2 [67, 68].

A quantitative estimate for the relaxation rate in a magnetic field was obtained by introducing a characteristic parameter τ [68] defined as the time corresponding to the factor-of-*e* deviation of the nonequilibrium Hall concentration from its stationary value. Using the parameter τ made it possible to see how the kinetics of the system tended to change as the alloy composition x, pressure P, and temperature T were varied. Increasing each of these variables led to a decrease in the parameter τ, but, for any value $H > H_{uql}$, x, T, and P, the parameter τ_1 was found to exceed τ_2 for inverse transitions.

This result is quite natural because the overflow of carriers from a level to a band is not equivalent to the reverse process. In a quantizing magnetic field, carriers are spin-polarized, making their energy spectrum quasi-one-dimensional. According to current views, some impurity centers in $Pb_{1-x}Sn_xTe(In)$ are occupied by two localized electrons with opposite spins. Thus, transitions from a level to a band must involve a reversal of the spin of one of the localized electrons. The inverse transition has no limitations on spin orientation.

The kinetics of the long-term relaxation process in a magnetic field proved to be rather complex. However, the very occurrence of a long-term magnetic-field-induced relaxation process in the metallic phase of $Pb_{1-x}Sn_xTe(In)$ suggests an important conclusion about the nature of the recombination barrier. The uniform electrical and physical characteristics of the crystals, the high mobility of their electrons, and the single-pole nature of the signal rule out the idea of this barrier being due to band-edge modulation. This leaves us with the specificity of impurity states as the main factor accounting for the long-term relaxation process in the alloy system being studied.

2.3.2 Long-term processes induced by IR illumination. IR illumination as an external influence enables one to produce the highest possible excitation levels in the electron subsystem. A high IR-illumination-induced photosensitivity at low temperatures was first found in $Pb_{1-x}Sn_xTe(In)$ alloys by Vul and coworkers [76]. Later, photoconductivity studies were made in Refs [77–83] on $Pb_{1-x}Sn_xTe(In)$ and in Refs [25, 29, 31, 78, 83–89] on PbTe(Ga).

The high photosensitivity of the $Pb_{1-x}Sn_xTe(In)$ and PbTe(Ga) systems required special measures to carefully screen samples from the background radiation when performing the experiment. For measurements under the conditions of controlled IR illumination, a liquid-helium-cooled metallic chamber was specially developed [77].

Figure 8 shows typical temperature dependences of the resistivity ρ of single-crystal PbTe(Ga) and $Pb_{1-x}Sn_xTe(In)$ ($x = 0.25$) samples measured in darkness (curves *1* and *2*, respectively) and with IR illumination (curves *1′* and *2′*). The temperature T_c, corresponding to the maximum in the IR curves, marks the onset of photoconductivity. For the $Pb_{1-x}Sn_xTe(In)$ alloys, the temperature T_c was about 20 K; for PbTe(Ga), about 80 K [78]. For $T < T_c$, the darkness and IR-illumination resistivities differed by several orders of

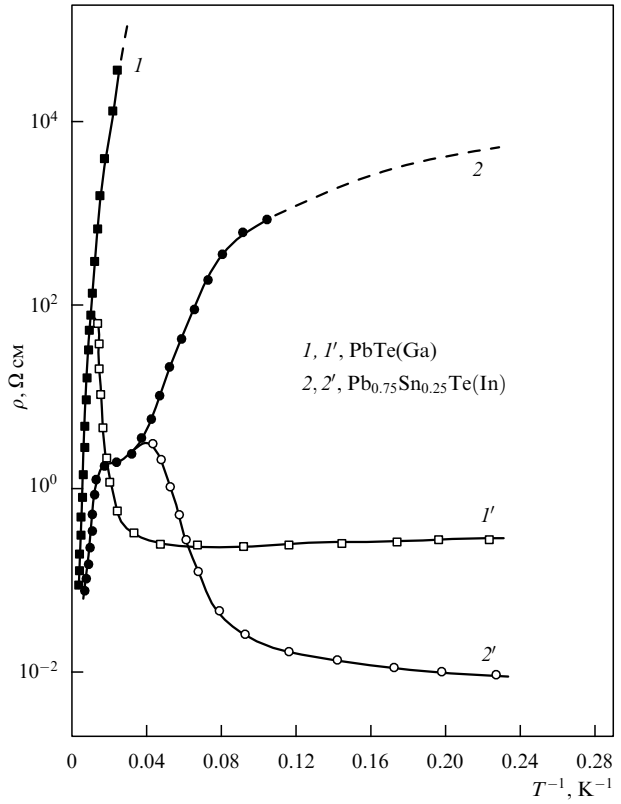

Figure 8. Temperature dependence of the resistivity ρ of PbTe(Ga) and $Pb_{0.75}Sn_{0.25}Te$(In) samples measured in darkness (curves *1* and *2*) and with IR illumination (curves $1'$ and $2'$) [78].

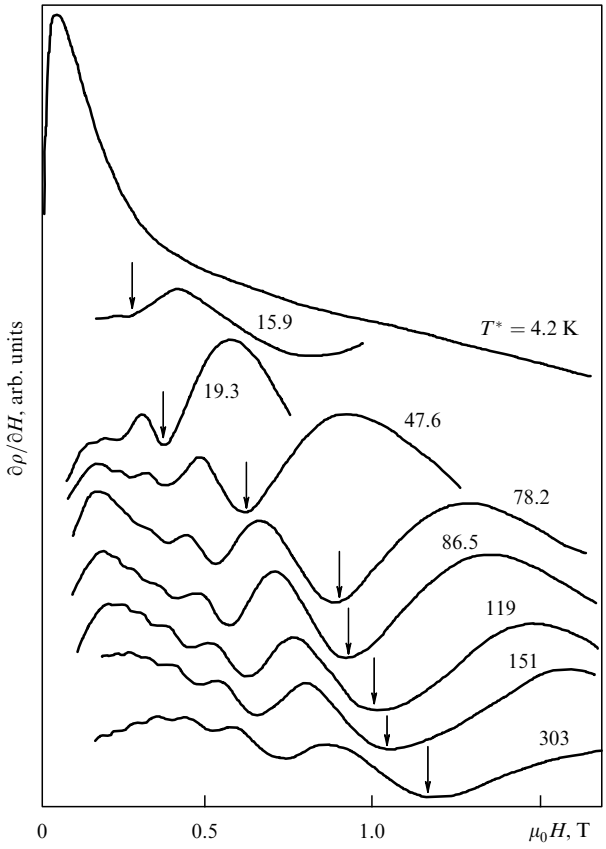

Figure 9. Oscillations of magnetoresistivity $\partial\rho/\partial H$ in the $Pb_{0.78}Sn_{0.22}Te$(In) sample under IR illumination at various temperatures T^* of the thermal radiation source. The arrows indicate the position of the extremum with a given quantum number, $T = 4.2$ K [77].

magnitude. Importantly, the parameter T_c was found to be independent of the composition x for the $Pb_{1-x}Sn_xTe$(In) alloys. Furthermore, also in photoconductivity studies on substitutional PbTe(In)-based solid solutions with other components (MnTe and GeTe) the temperature T_c was found to differ little from 20 K. In the same solid solutions doped with gallium, T_c remained close to 80 K.

A nonequilibrium state induced by IR illumination was observed both in the semi-insulating ($0.22 < x < 0.28$) and the metallic ($x < 0.22$, $x > 0.28$) phases of the $Pb_{1-x}Sn_xTe$(In) alloys. The appearance and increase of the Fermi surface is nicely illustrated by Shubnikov – de Haas oscillations recorded at various excitation levels [68]. Figure 9 presents the magnetic-field derivative of magnetoresistivity $\partial\rho/\partial H$ for the $Pb_{1-x}Sn_xTe$(In) ($x = 0.22$) sample. As a thermal source for IR illumination, a carbon resistance was used, which was heated to a certain temperature T^* by the current passing through it. As the temperature T^* of the thermal source was increased, the concentration of nonequilibrium electrons began to grow slowly.

Each of the curves in Fig. 9 corresponds to a certain quasi-stationary electron concentration existing under the IR illumination conditions. The oscillations shown were recorded after the generation and recombination processes have become comparable in rate. When the IR illumination was turned off, the electron concentration decreased slowly. The process of slow contraction of the Fermi surface was illustrated by recording oscillation curves, whose period changed with time [67]. The experiments described convincingly demonstrate the existence of a recombination barrier between the localized and free electron states and leave no doubt about the crucial role of impurity states in its formation.

The nonequilibrium electron concentration induced by IR illumination in the $Pb_{1-x}Sn_xTe$(In) alloys reached $10^{17}-10^{18}$ cm^{-3} — values that had been unachievable in magnetic-field experiments.

The kinetics of the relaxation of conductivity to its equilibrium value σ_{st} in the $Pb_{1-x}Sn_xTe$(In) alloys has been studied in detail in Refs [77, 79 – 82]. The $\sigma(t)$ dependences were found to be rather complex and not describable by an exponential law with a single characteristic relaxation time τ.

To interpret the experimental data, various approaches have been employed. The authors of Ref. [81] approximated the $\sigma(t)$ curves by two exponential functions with differing exponents. Ref. [82] proposes a phenomenological equation involving an exponential functions in which the exponent itself is a function of time. This dependence of the time τ implied that the quasi-Fermi level shifts in the process of relaxation. In Ref. [79], persistent photoconductivity was approximated by a logarithmic function, and in Ref. [77], by a power law. All these approximations fully discredited the idea of describing the entire relaxation process by a single simple equation. Choosing limited regions in the $\sigma(t)$ curve, it is likely possible to provide more freedom in choosing an approximating function.

Additional uncertainty in the interpretation of relaxation processes is due to the fact that the rate of relaxation depends on the excitation level involved. Kinetic processes also depend

to a large extent on the content of indium in the solution, even though the concentration of electrons in a stationary state remains constant [90].

Relaxation processes in $Pb_{1-x}Sn_xTe(In)$ alloys of varying composition x subject to thermal radiation from an ohmically heated carbon resistance were studied in Ref. [77]. The conductivity saturation level, $\sigma(t \to \infty)$, for a fixed thermal source temperature T^* was found to depend in a nonmonotonic way on x. The conductivity $\sigma(t \to \infty)$ reached its maximum at $x = 0.26$, which corresponded to the Fermi level being located close to the middle of the energy gap. For the same composition, the fastest relaxation rate was observed.

The kinetics of photoconduction in PbTe(Ga) alloys turned out even more complex. Consistent with Refs [85, 86], the lifetime τ_h of nonequilibrium holes at $T = 77$ K was below 10^{-8} s, whereas the electron lifetime τ_e was of order 10^{-3} s. Reducing the temperature produced two distinct regions in the kinetic curves: a relatively fast process immediately after the IR illumination is turned off, and a virtually frozen photoconductivity some time later. At liquid-helium temperature, characteristic times for the slow process exceeded 10^5 s. Note, however, that this is just an estimate for the lower limit on τ rather than a typical value.

The relationship between the nonequilibrium carriers participating in the fast and slow processes depends on many parameters, including the duration and intensity of IR illumination [12]. This conclusion was drawn based on the study of photoconductivity kinetics in single-crystal samples of PbTe(Ga) exposed to radiation from a laser, a light-emitting diode, and a thermal source [91].

Qualitative features of the relaxation process in single-crystal samples were subsequently reproduced in semi-insulating epitaxial films of *n*-PbTe(Ga) with thicknesses in the range of 0.2 to 2.0 μm [87, 88]. Figure 10a illustrates relaxation kinetics for a film about 1 μm thick exposed to IR illumination pulses at various light flux densities. The characteristic features of both curves are that the photoconductivity signal rapidly increases after the thermal source is turned on, rapidly drops to a certain intermediate level after it is turned off, and increases virtually at the same rate to the originally achieved level when the thermal source is turned on again.

The kinetics of photoconductivity in the same film for IR illumination by a light-emitting-diode ($\lambda = 1$ μm) is shown in Fig. 10b. Persistent photoconductivity was observed for light-diode pulse durations above 10 ms. Such kinetics is observed when nonequilibrium electrons can be trapped by at least two types of centers differing in the height of the recombination barrier. The fast process is determined by the lower-barrier centers (metastable impurity states), whereas long-term relaxation processes involve higher-barrier centers (the ground state of an impurity) [87]. The nonexponential behavior of the nonequilibrium processes may be due to the fact that a change in the concentration of nonequilibrium carriers is accompanied by a change in the concentration of impurity centers in certain charge states.

Important information about kinetic processes was obtained from a comparative study of films of different thicknesses. The drop in the conductivity $\sigma(t)$ following the passage of a light-emitting-diode IR illumination is shown in Fig. 11a for PbTe(Ga) films with thicknesses $d = 2$ μm and $d = 0.2$ μm (the duration of the IR pulse was 10 ms, $T = 4.2$ K; the zero of the time scale is at the end of the IR illumination).

The qualitative differences between the samples with different thicknesses are quite understandable. First, the thick film of *n*-PbTe(Ga) relaxes to equilibrium much faster than the thin one. Second, the kinetic curve for the thick film is not rectifiable in the $\log\sigma$-vs.-t coordinates, unlike the thin-film photoconductivity, for which classical exponential kinetics is observed virtually at all times except for a short period at the very beginning of the relaxation curve.

This result is neatly illustrated by the kinetic dependences of the instantaneous relaxation time $\tau(t)$ shown in Fig. 11b. For the thin film, the relaxation time τ rapidly (within $t < 10$ ms) reaches the value 13 ms and then remains virtually

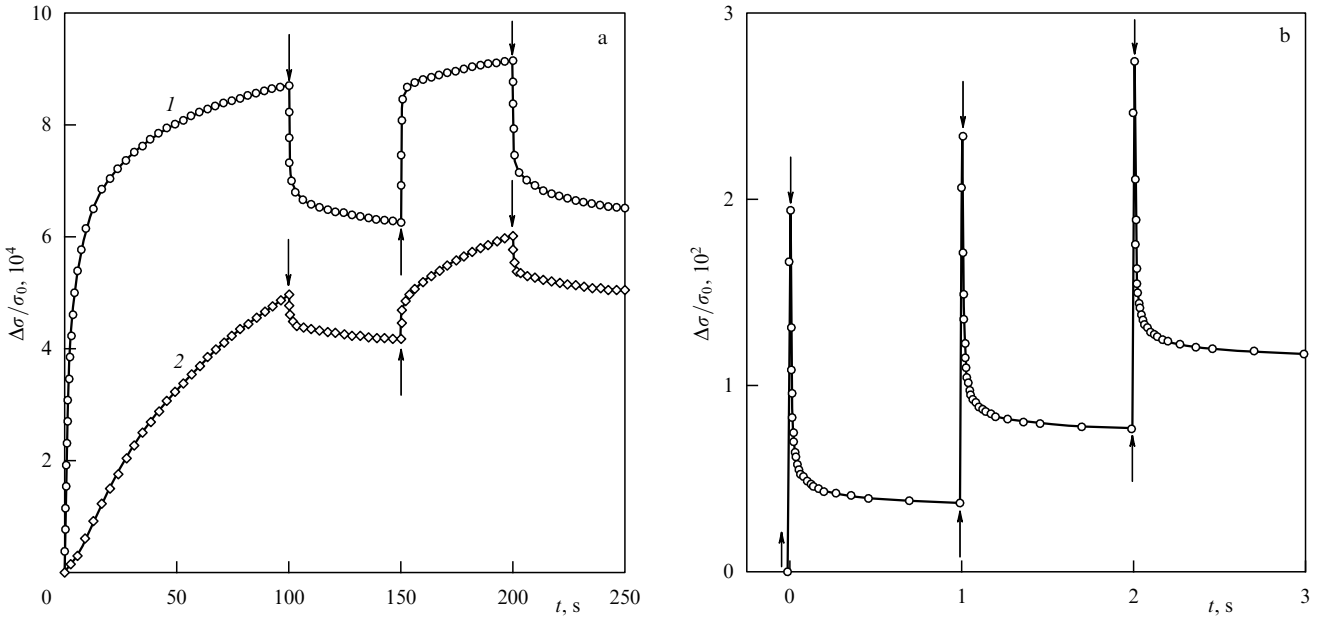

Figure 10. Kinetics of photoconductivity $\Delta\sigma/\sigma = (\sigma - \sigma_0)/\sigma_0$ (σ_0 is conductivity at $t = 0$) for an *n*-PbTe(Ga) film on a BaF_2 substrate under IR illumination [87]: (a) thermal radiation source, light flux density 10^{-5} W cm^{-2} (curve *1*) and 10^{-6} W cm^{-2} (curve *2*); and (b) light-emitting diode, $\lambda = 1$ μm, pulse duration 10 ms. The arrows indicate turning IR illumination on (↑) and off (↓). $T = 4.2$ K.

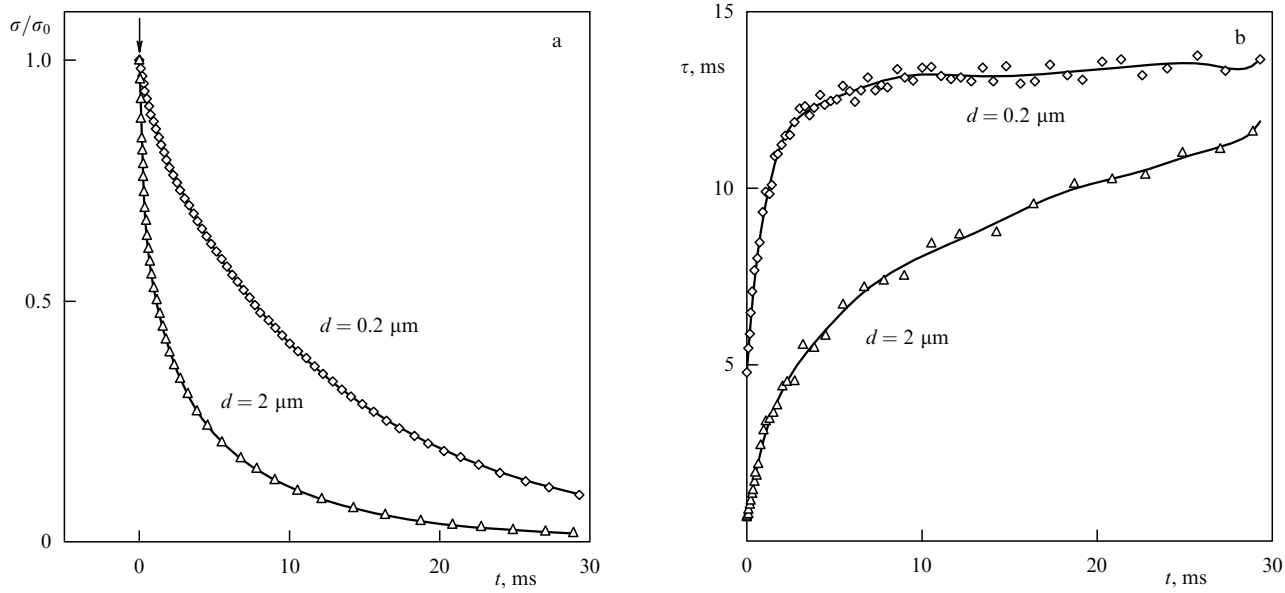

Figure 11. (a) Photoconductivity $\sigma(t)$ and (b) instantaneous relaxation time $\tau(t)$ of nonequilibrium charge carriers as functions of time following the turn-off of IR illumination in *n*-PbTe(Ga) films of different thickness [88].

unchanged. The curve $\tau(t)$ for the thick film is characterized by a continuous growth of τ throughout the entire relaxation process; its asymptotic limit may correspond to the same value $\tau = 13$ ms observed in the thin-film case [88].

The results indicate that the diffusion of nonequilibrium carriers from the surface inward considerably affects the shape of the relaxation curves for bulk samples. In analyzing relaxation processes, one should take into account that in *n*-PbTe(Ga) alloys, slow processes dominate under high excitation conditions, and relatively rapid relaxations are observed under weak pulsed IR illumination. This may be due to the fact [87] that at high concentrations of nonequilibrium electrons the number of metastable impurity centers is small in comparison with the number of impurity centers in the ground state.

The diffusion of nonequilibrium electrons deep into the crystal offers an additional possibility that the electrons may 'find' a metastable center and recombine there. The diffusion process is likely to be important not only in bulk single crystals but also in films about 2 μm thick. This may explain the lower value of $\tau(t)$ for the thicker films. Given that an exponential transient kinetics is observed only in the thinnest films studied, it is reasonable to assume that it is only there that excitation is uniform throughout the volume.

Another important result obtained in the study of PbTe(Ga) is that the parameter T_c, characterizing the onset of photoconductivity, increases markedly as the film thickness decreases. While in bulk samples the temperature T_c is about 80 K, in films with a thickness of 1 μm it increases to 110 K, and in thin films (0.2 μm in thickness) it reaches 150 K. Interestingly, the thin films showed very extended linear regions in the dependences of log $(\rho_{\text{illum}}^{-1} - \rho_{\text{dark}}^{-1})$ on the inverse temperature. Assuming that at sufficiently high temperatures ($T > 50$ K) the recombination rate of nonequilibrium carriers $\delta R \propto (\Delta n)\tau$ at each point equals the generation rate (which remains constant under experimental conditions) and assuming that the characteristic time for the slow recombination process is $\tau \propto \exp(W/kT)$, the estimate for the recombination barrier is $W = 26.5$ meV [88].

The epitaxial films of $Pb_{1-x}Sn_xTe$(In) ($0.19 < x < 0.23$) [92–95] and PbTe(Ga) [89] show negative photoconductivity. In $Pb_{1-x}Sn_xTe$(In), negative photoconduction was observed on samples illuminated by semiconductor lasers in combination with background illumination. In this case, the effect can be interpreted by assuming that the negative photoconductivity induced by background illumination is quenched by laser pulses with a quantum energy exceeding E_g.

In PbTe(Ga) samples, the conduction band contained electrons even under darkness conditions, because in the films under study the concentration of donor gallium was in excess of that needed for the stabilization of the Fermi level. Since the characteristic recombination times for negative photoconductivity proved to be much less than those known for modulated-band-edge systems (in PbTe(Ga) at $T = 4.2$ K, τ measures tens of milliseconds), this effect suggests that in both cases the energy spectrum of the alloy contains an additional level above the conduction-band bottom.

In summary, in lead telluride-based alloys, indium and gallium behave as mixed-valence impurities, creating a system of levels corresponding to various charge states of the impurity. A detailed analysis of relevant theoretical concepts that have been developed until now is given in Section 3 following a discussion of basic experimental results.

2.4 Strong electric field phenomena. Hot electrons

The current – voltage ($I-V$) curves of undoped lead telluride in strong electric fields has an extended sublinear region followed by a region of negative differential conductivity of *N* or *S* type [96–98]. On the decreasing branch of an $I-V$ curve high-field domains and current instabilities are seen [97, 99, 100]. These effects are attributed to the Gunn effect, due to an additional extremum in the conduction band. The threshold field E_{th} for instabilities is sufficiently large: for example, in *n*-PbTe it reaches 1.5 kV cm^{-1} [98].

According to Refs [96, 98, 101], 'conventional' impurities do not affect the value of E_{th}, thus supporting the Gunn-effect interpretation of instabilities. Doping $Pb_{1-x}Sn_xTe$ alloys with indium significantly affects both the shape of the $I-V$ curves

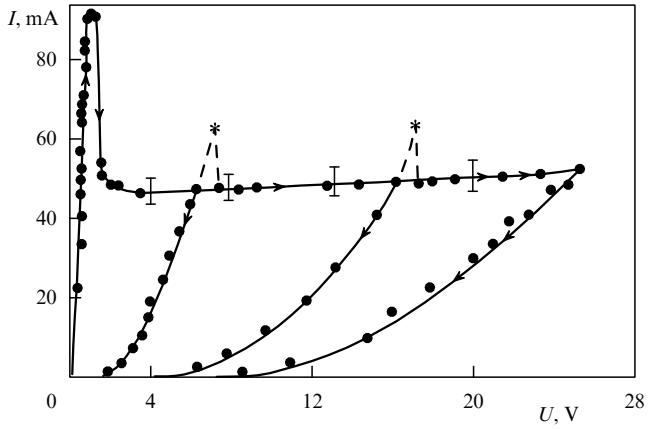

Figure 12. $I-V$ curves of the n-$Pb_{0.79}Sn_{0.21}Te$(In) sample (metallic state). The length of the sample is 0.25 cm [102].

and the domain parameters. The properties of nonequilibrium charge carriers in strong electric fields were studied [102] on single-crystal samples of $Pb_{1-x}Sn_xTe$(In) in the metallic phase with a conductivity of n and p type ($x = 0.2$ and $x = 0.3$, respectively). The impurity concentration was sufficient to stabilize the Fermi level.

Nonlinear $I-V$ curves, regions with N-like negative differential conductivity, and the appearance of high-field domains were observed at electric fields below 10 V cm^{-1}, which is two order of magnitude less than in undoped samples. The $I-V$ curves showed strong hysteresis in an n-type sample. An N-like branch was detected only with the field turned on (Fig. 12). The turn-off branches lie markedly lower, so that the conductivity of the sample drops off sharply following the passage of an electric field pulse. The relaxation of conductivity to the initial value is slow. In p-type samples the field strength corresponding to the N-like region of the $I-V$ curve is somewhat higher (20 to 40 V cm^{-1}), and no hysteresis is observed.

High-field domains in $Pb_{1-x}Sn_xTe$(In) samples differ from Gunn's domains. The velocity of the domains depends on the value of the applied field. Close to the threshold field E_{th}, the velocity is 10^2 cm s^{-1}, and it increases to 10^6 cm s^{-1} as the field strength increases to 40 V cm^{-1} [102]. A domain does not disappear immediately after the field is turned off but instead survives for tens of minutes at liquid-helium temperature. Hall effect measurements showed that the carrier concentration in the vicinity of a domain is much lower than in the sample in the stationary state, but the mobility remains unchanged. The most plausible explanation of domain instability in $Pb_{1-x}Sn_xTe$(In) samples is that hot electrons are trapped by indium impurity states. Large domain lifetimes confirm the presence of a recombination barrier between the band and localized states.

Static $I-V$ curves for semi-insulating samples of $Pb_{1-x}Sn_xTe$(In) at $x = 0.25$ were studied in Ref. [102]. The $I-V$ curve at small currents under screening conditions had the form $I \propto E^2$. One of the factors determining the $I-V$ curve could be the monopolar injection of carriers from contacts to the semi-insulating sample. In Ref. [104] this region of the $I-V$ curve was associated with a ferroelectric phase transition [105, 106].

In the region of large fields, the $I-V$ curve has an S-like region, possibly due to an electrothermal breakdown [103, 107]. Under IR illumination, an additional N-like region was

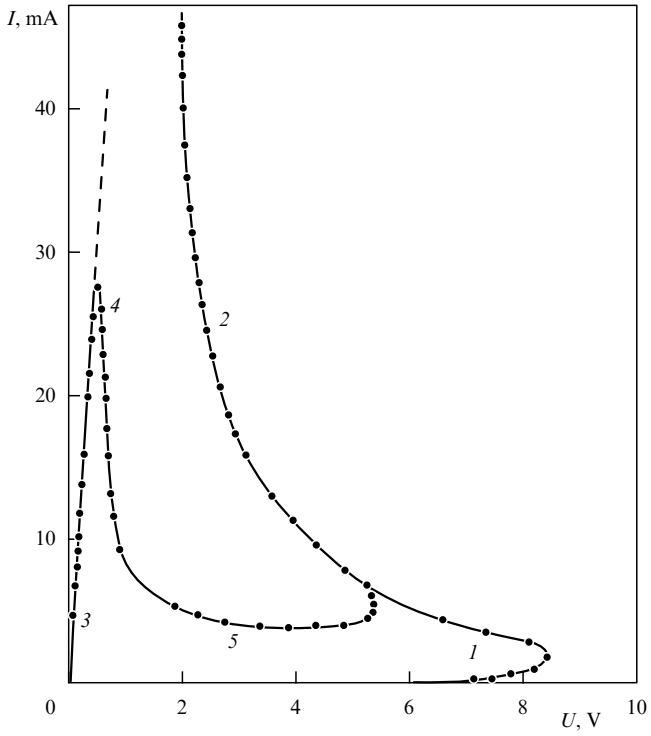

Figure 13. Static $I-V$ curves of the $Pb_{0.75}Sn_{0.25}Te$(In) sample (insulating state) in darkness (regions *1*, *2*) and under IR illumination (*3*–*5*). The sample length is 0.29 cm [103].

observed in low fields (Fig. 13). The heating of electrons in the electric field caused an increase in the capture rate and a decrease in the electron concentration n, and led to a negative differential conductivity. These results were also reproduced in a study of $Pb_{1-x}Sn_xTe$(In) thin films with $x = 0.22$ [108].

The $I-V$ curves of PbTe(Ga) samples were studied between 4.2 and 170 K in pulsed fields up to 3000 V cm^{-1}, with pulse duration varying from 0.03 to 40 μs [109]. The linear region was observed only for $T > 70$ K in very low fields $E < 1$ V cm^{-1}. In fields from 100 to 400 V cm^{-1}, the shape of the $I-V$ curve corresponded to the Poole–Frenkel mechanism $\ln I \propto E^{1/\gamma}$, with $\gamma = 1.9-2$. In fields from 300 to 1000 V cm^{-1}, an electron breakdown was observed, with a conductivity increase by 10^7 to 10^8 times at $T = 4.2$ K. The lifetime of nonequilibrium carriers produced in the breakdown exceeded 10^5 s at liquid-helium temperatures and decreased to 10^{-2} s at $T = 77$ K.

Under hydrostatic pressure, the behavior of semi-insulating samples in high electric fields is qualitatively different [110]. For $P \geqslant 1.5 \times 10^9$ Pa, a sample in a pulsed field shows a reverse response, i.e., changes to a lower-conductivity state. The conductivity drop reaches two orders of magnitude, and relaxation times increase. In Ref. [110] this is explained by the stabilized Fermi level shifting to the valence band at $P > 1.5 \times 10^9$ Pa. The low-temperature low-field conductivity is then dominated by the holes in the valence band. In high fields, hole localization on impurity centers takes place, and the conductivity falls off.

2.5 Optical absorption

Optical absorption experiments provide direct information on the energy spectrum of impurity states. However, experimental results may be difficult to interpret if a semiconductor

is doped with mixed-valence impurities, which form a system of impurity levels with recombination barriers between them, in the semiconductor's energy spectrum. Due to the barrier between electron free and localized states, an experimentally determined energy of a direct optical transition may differ from the energy of the corresponding impurity level as measured from the edge of the nearest allowed band.

There are also methodological problems due to the high photosensitivity of some materials (see Section 4.2) at sufficiently long wavelengths in the infrared. To perform spectral measurements at low temperatures with the background illumination screened out is all but impossible. Hence, long-term relaxation processes are studied in materials that are *a priori* in a nonequilibrium state.

Optical absorption studies have been made on lead telluride doped with Group III elements: B [111], Al [112], In [113], Ga [28], Tl [114]. In all cases, only resonance levels showing energy correspondence with the dopant's atomic number were observed. The heavier the impurity atom, the lower the energy of the corresponding level. At $T = 300$ K, the B, Al, and Ga levels are high in the conduction band, the level of In is closer to its bottom, and the level of Tl falls within the valence band. It is quite likely that the energy position of the resonance gallium level detected from absorption spectra corresponds to one of the saturation regions on the $n, p(N_{Ga})$ dependence in the high impurity concentration range [28].

In $Pb_{1-x}Sn_xTe$(In) alloys, an additional absorption is observed beyond the edge of the fundamental band [113, 115–117]. This absorption was attributed to conduction-band–impurity-level transitions in the case of a resonance level ($x < 0.22$) and to reverse transitions in the case of a local level ($0.22 < x < 0.28$). Because the spectra were recorded at $T = 77$ K, no features due to persistent photoconductivity were observed. Later, measurements at helium temperature were also made [93]. The spectra were found to be complex, and the optical absorption to decrease in time. Optical transitions between the ground and metastable impurity states were proposed as an explanation.

The authors of Ref. [93] associated the long-term nature of relaxation with a barrier, in configuration-coordinate space, between the ground and metastable states of the impurity center. According to their estimates, the concentration of metastable states was much lower than the total amount of impurity in the sample. It was suggested therefore that the observed states may originate not from an isolated impurity atom but rather from complexes containing an impurity atom and a crystal-lattice defect.

Ref. [118] reports a sharp optical absorption peak in the $Pb_{0.78}Sn_{0.22}Te$(In) alloy at a frequency $\omega_{loc} = 160$ cm^{-1}. The peak corresponds to a local mode of In in the crystal lattice of $Pb_{1-x}Sn_xTe$(In) alloys.

2.6 IR refection and Raman scattering spectra

Experimental data on reflection spectra show that the persistent photoconductivity effect leads to an increase in plasma frequency [119–122]. The major features of reflection spectra are in good agreement with galvanomagnetic measurements. However, the results of Ref. [120] show that hydrostatic pressure has little effect on photoresponse, which is inconsistent with the conclusion of Ref. [123] that pressure speeds up relaxation in a magnetic field.

According to Ref. [124], at temperatures below $T_c = 25$ K an additional structure is observed in the reflection spectra of $Pb_{0.75}Sn_{0.25}Te$(In) alloys. (T_c marks the onset of persistent photoconductivity.) The description of this structure requires introduction of an additional oscillator to the dispersion relation. The frequency of the oscillator is $\omega_0 \approx 120$ cm^{-1}, and its strength increases at $T < T_c$ and saturates at $T < 10$ K. A similar structure was observed in the absorption spectra of PbTe(Ga) [125]. In that experiment, the oscillator strength increased at $T < T_c = 80$ K, and its frequency ($\omega_0 \approx 155$ cm^{-1}) was much higher than for indium-doped alloys.

Since the ground state of an impurity must manifest itself over the entire temperature range, the observation of an oscillator in a limited temperature range was explained by the introduction of an additional vibration mode due to local metastable one-electron states E_1. An important point is that a simple relation between local modes

$$\frac{\omega_0(\mathrm{Ga})}{\omega_0(\mathrm{In})} = \left(\frac{m_{\mathrm{In}}}{m_{\mathrm{Ga}}}\right)^{1/2}, \tag{2.2}$$

in which only the mass difference between the indium and gallium atom is taken into account is valid in this case.

Another important result is that the oscillator strength grows at temperatures $T < T_c$. This indicates a sharp increase in the density of states with energy E_1 just in the temperature range where persistent photoconductivity is observed. It is suggested [127] that the barrier between the ground (two-electron) and metastable (one-electron) impurity states in the configuration-coordinate space disappears at $T = T_c$, as disappear the metastable states themselves. This conclusion requires further justification, however, in view of the fact that later photoconductivity studies of epitaxial PbTe(Ga) films show a significant (up to 150 K) increase in T_c in films about 0.2 μm thick [88].

Experimental studies of Raman scattering spectra in PbTe(In) [126] provide additional information on the microscopic structure of a metastable impurity center. At $T < 100$ K, an active Raman mode with a frequency of about 115 cm^{-1} was clearly observed. The amplitude of the Raman peak increased strongly at $T < 25$ K but remained too weak compared to the active modes of the crystal lattice itself. This points to local distortions of inversion symmetry as the origin of the active Raman mode.

As indicated above, the local modes of indium and gallium are related by Eqn (2.2). It is natural to assume that since indium and gallium are substituted for lead in the crystal lattice, the relation

$$\frac{\omega_0(\mathrm{Ga})}{\omega_{\mathrm{LO}}} = \left(\frac{m_{\mathrm{Pb}}}{m_{\mathrm{Ga}}}\right)^{1/2} \tag{2.3}$$

holds. This proved not to be the case, however. This apparent inconsistency can be resolved by assuming that atoms in a metastable state are displaced relative to the crystallographic position of lead in the lattice. The strain constants may then change, making Eqn (2.3) invalid [127].

It is well known that in III–V semiconductors the ground state of a DX-center corresponds to an impurity atom displaced from its site, whereas a shallow excited metastable state corresponds to an on-site impurity atom [75]. An important conclusion reached in Ref. [127] is that, in IV–VI semiconductors, it is an impurity atom in a metastable state that is displaced. At the same time, an atom in its ground state — as well as an atom with an unfilled outer electron shell — most likely do occupy sites in the metal sublattice.

2.7 Photoconductivity spectra

In Section 2.5 we mentioned methodological difficulties that arise in the optical absorption studies of highly photosensitive lead telluride-based alloys doped with indium and gallium. Those difficulties apply equally well to studies of photoconductivity spectra. Using standard instruments, it is in principle impossible to screen a sample fully from the background radiation from those parts of the equipment that are at room temperature. Thus, direct measurements of photoconductivity spectra can only be performed on a sample that is *a priori* in a nonequilibrium state.

In interpreting experimental results, an important point to remember is that, due to the Franck–Condon effect, the recombination barrier between the band and localized states should create a difference between the optical and thermal activation energies. In Ref. [128], a specially designed calculation method was used to estimate the optical activation energy for $Pb_{1-x}Sn_xTe(In)$ alloys under conditions of screened-out background radiation and controlled blackbody illumination. The result was surprising in that the optical activation energy proved to be equal to the thermal one. This was explained by assuming that the energy of the longitudinal optical phonon was close to the thermal activation energy of the carriers.

The photoconductivity spectra of $Pb_{1-x}Sn_xTe(In)$ ($x > 0.22$) alloys at low temperatures were studied in Refs [129–134] using standard spectroscopy instruments. The composition x corresponding to the metallic state of the alloys was chosen to minimize the effect of background illumination. While photoconductivity beyond the edge of the fundamental band is reported in all of the studies, a structure with an impurity photoconductivity band in this spectral region was observed only in Refs [129, 130]. The band, described by the Gaussian distribution, was attributed to transitions between the ground and metastable local states of impurities.

It should be noted that this result is one of the first pieces of evidence for the existence of metastable states in $Pb_{1-x}Sn_xTe(In)$. Still, it was not entirely clear how transitions between two localized states may contribute to photoconduction. A possible explanation is that photoexcitation creates an excessive population of metastable impurity states located in the immediate vicinity of the conduction-band bottom and separated by a low barrier from the allowed states. In this case, the thermal or optical excitation due to the background illumination can delocalize an electron.

The data on epitaxial films of $Pb_{1-x}Sn_xTe(In)$ ($0.19 < x < 0.23$) [92–95] are apparently the most correct data experimentally. Photoconductivity spectra were recorded in darkness or with background illumination being controlled. The radiation sources used were lasers at a fixed far-infrared wavelength. Perhaps the most interesting finding is negative photoconductivity (earlier mentioned in Section 2.3.2). Results were explained in terms of metastable quasi-local one-electron states separated by energy barriers (in the space of configuration coordinates) both from the band states and from the two-electron local ground states. The analysis of various optical transitions between these states suggests [92, 94, 95] that negative and positive photoconductivity cannot coexist unless metastable one-electron states exist.

Most studies on the photoconductivity spectra of PbTe(Ga) alloys have been performed at $T \geqslant 77$ K, i.e., close to T_c. The major finding of these studies is that no measurable photoconductivity is found beyond the edge of the fundamental band. This seemed strange, to say the least, because the temperature dependences of the galvanomagnetic coefficients clearly revealed an impurity level close to the middle of the forbidden band [12].

However, in the immediate neighborhood of the absorption edge a sharp photoconductivity peak was observed by a number of workers [84, 135, 136]. The peak was originally treated as an intrinsic spectral feature. An analysis in Ref. [137] revealed the impurity nature of the peak: it was explained by an intracenter transition on an impurity atom. According to the data of Ref. [138], the relative amplitude of the peak depends on the method used to prepare PbTe(Ga) crystals. In PbTe(Ga) films, the structure of the absorption band is well described by the relation for undoped PbTe, the amplitude of the additional peak is small, and its position corresponds to the energy of a level located 20 meV below the conduction-band bottom.

A resonance structure was also observed in a spectral study of the fast photoconductivity component in PbTe(Ga) and its solid solutions [139]. The photoconductivity peak was at an energy corresponding to intrinsic absorption and shifted together with the edge of the fundamental band as the temperature and composition of an alloy were varied (Fig. 14). The resonance structure was explained by optical transitions from the valence band to a metastable local one-electron state close to the conduction-band bottom. This result is a strong argument in favor of a model [140] that allows for localization of a p electron in the short-range potential of an empty (s^0p^3) impurity center (see Section 3).

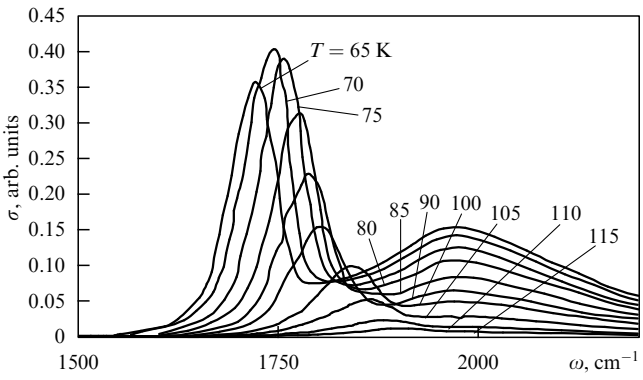

Figure 14. Photoconductivity spectra of a PbTe(Ga) sample in the midinfrared [139].

PbTe(Ga) also was found to display a selective photoresponse in the far infrared at $\omega_0 = 155$ cm^{-1} [139], which is exactly the oscillator frequency observed in reflection spectra. This line in the photoconductivity spectrum is due to the optical excitation of the local vibration mode corresponding to metastable states of the impurity. A more detailed discussion of the behavior of the photoconductivity of PbTe(Ga) in the far infrared is given in Section 4.4.

2.8 Tunneling spectroscopy

Tunneling spectroscopy employs nonequilibrium carriers with a fixed energy and is therefore one of the most informative techniques that determine the structure of the density of states and the energy positions of quasi-local levels.

Kaĭdanov and coworkers [42, 141–143] used tunneling spectroscopy to study PbTe doped with indium or gallium.

The tunneling structures $Pb/Al_2O_3/PbTe$ or Pb/ZnS/PbTe were prepared using bulk single crystals of either doped or undoped lead telluride. By applying a quantized magnetic field and observing the quantum oscillations of the tunneling current, the researchers determined the relation between the applied bias and the energy of the injected electrons as measured relative to the edges of the allowed bands of PbTe.

The $I-V$ curves of both doped and undoped structures were found to feature a peak. The position of the peak corresponded to the edge of the second valence subband. Doping with thallium produced yet another peak, one associated with quasi-local thallium states. The energy position of the peak was close to the value derived from Hall-coefficient measurements. The analysis of the peak's shape supported the assumption that the broadening of an impurity level is due to the hybridization of the band and impurity states.

In the case of indium doping, the situation is qualitatively different. Instead of a peak, a hysteresis and oscillation features appear in the $I-V$ curve [141]. The data are interpreted by assuming metastable (one electron on an impurity center) and ground (two electrons on an impurity center) impurity states to be present in the system. According to calculations, the metastable impurity level in PbTe(In) is 35 meV above the ground level that stabilizes the Fermi level. The Coulomb repulsion of the two electrons residing on an impurity center is estimated to be 60 – 70 meV.

The estimate of the relative energy positions of the ground and metastable states appears to be indirectly confirmed by photoconductivity-kinetics studies on $Pb_{1-x}Mn_xTe$(In) for different x [144]. Based on the parameters obtained in Ref. [141], it is established that the qualitative change in the nature of relaxation occurs in the composition (x) range corresponding to the metastable state being shifted to the forbidden band.

2.9 Magnetic properties

A paramagnetic contribution to the magnetic susceptibility χ, if discovered, would argue strongly in favor of the existence of metastable one-electron impurity centers in lead telluride-based solid solutions doped with Group III elements. While this contribution has been found [9] in PbTe(Tl), measurements of the magnetic susceptibility χ in PbTe(In) with a stabilized Fermi level showed no paramagnetic signal [145]. This confirms that the ground state of an impurity center is a state with two electrons localized on the center.

Experimental studies of the magnetic properties of lead telluride with magnetoactive dopants proved to be more informative. Story and coworkers performed electron paramagnetic resonance (EPR) and magnetization studies on lead telluride doped with Cr [18, 21, 63, 146], Gd [62], and Yb [56, 59]. The experiments confirmed the view that the valence of the impurities is variable. The magnetic properties are fully consistent with the way the carrier concentration depends on the impurity content. The saturation regions in the $n(N_i)$ dependences are accompanied by the stabilization of magnetic characteristics. Unlike the elements of Group III, the magnetoactive state of chromium and rare-earth elements — the state that contributes to the EPR signal — is a donor state with a charge 3^+. Thus, magnetic measurements in this case make it possible to control the concentration of electrically active impurity centers.

A very unusual result was obtained in a study of the magnetic susceptibility of PbTe(Ga) in the temperature range 4 – 100 K [147]. The measurements were made by the Faraday method in magnetic fields of up to 1 T. Importantly, the sample was not fully screened from the background illumination in the process of measurement. In the temperature range of 50 – 70 K, the $\chi(T)$ dependence exhibited a sharp paramagnetic peak. At $T < 45$ K, the paramagnetic contribution to the magnetic susceptibility followed the Curie – Weiss law with a characteristic temperature of $\theta = -5.8$ K. The negative value of θ indicated the antiferromagnetic nature of the exchange interaction in the impurity – impurity system. It was suggested that the paramagnetic signal was due to electron localization on paramagnetic centers (p electrons localize in the potential of an impurity state with configuration s^0p^3) [127, 140].

2.10 Thermally stimulated currents and photoresponse instabilities

Thermally stimulated currents are usually observed in semiconductors with impurity levels within the forbidden band. The standard technique of thermal-activation current spectroscopy was employed in the study of thermally stimulated currents in the single crystals of $Pb_{1-x}Mn_xTe$(In) and PbTe(Ga) and the epitaxial films of $Pb_{1-x-y}Sn_xGe_yTe$(In) in the temperature range of 4.2 – 30 K [148, 149]. The most accurate picture of the peaks of thermally stimulated currents was obtained for films of $Pb_{1-x-y}Sn_xGe_yTe$(In) with an impurity-conduction activation energy E_a of less than 50 meV. For the crystals of $Pb_{1-x}Mn_xTe$(In), the peaks of thermally activated currents were observed only in samples with $x = 0.07-0.08$ ($E_a = 40$ meV). It should be noted that this is precisely the composition for which the metastable impurity level turns out to be shifted into the forbidden band [144].

A feature of the materials studied is that thermally stimulated currents show peaks at the temperature T_m varying from 5 to 14 K, i.e., at much lower temperatures as compared to classical and wide-bandgap semiconductors. For PbTe(Ga), the peaks proved to have a more complex structure: a set of peaks of different amplitudes were observed at temperatures below $T_c = 80$ K.

In Refs [148, 149] the peaks of thermally stimulated currents are explained by the thermal excitation of carriers from a metastable impurity level to the conduction band. However, no explicit correlation has been found between T_m and the activation energy E_a — due to difficulties in experimentation and for fundamental reasons. Experimentally, there are quite a number of factors that affect the position of the peak but are difficult to control. Besides, the generation and recombination of nonequilibrium carriers are accompanied by the redistribution of the charge states of impurity centers.

Thus, the concentration of trapping centers changes in the course of an experiment and depends on its ordering. This means that varying the illumination intensity and temperature in different ways one can obtain the same conductivity in samples with different relations between the metastable and ground impurity centers. The experimentally discovered electrical instabilities of photoresponse may be considered as an indirect confirmation of this assumption. An example of such instability is considered in Ref. [149]. A film of $Pb_{1-x-y}Sn_xGe_yTe$(In) was originally illuminated by a low-intensity thermal source of radiation at a temperature $T = 4.2$ K. On a repeated turn-on of illumination of the same intensity at a certain intermediate stage of relaxation

to the darkness state, the film proved to be fully insensitive to illumination. As the sample was further heated to 6 K, a photocurrent was found to appear rapidly.

Another experimental confirmation of the existence of metastable states has come from the study of electrothermal instabilities (self-excited vibrations and waves) in PbTe(Ga) [150]. The idea of the experiment is as follows: the energy spectrum of PbTe(Ga) features two impurity levels, one of which (the ground level) lies somewhat above the middle of the forbidden band, and another (metastable level) under the conduction-band bottom. Together with the conduction band, this makes a three-level system. If illumination creates nonequilibrium carriers by exciting them from metastable states and if the applied electric field is sufficient to cause an electrothermal breakdown, periodic electric current and temperature oscillations will be observed in the system. An increase in the current is accompanied by a temperature growth. At a certain critical temperature, the recombination of nonequilibrium carriers from a metastable state to the ground state becomes a dominant process, the electron concentration decreases, the current drops, and the sample ceases to be heated. The cycle is then repeated.

Periodic current oscillations at $T = 4.2$ K and a bias $U = 35$ V are shown in Fig. 15a (the sample is $3.0 \times 0.8 \times 0.5$ mm in size). The way in which the nature of the oscillations depends on experimental parameters is illustrated in Figs 15b–15e. Figure 15b corresponds to an increase in helium pressure in the measurement chamber (heat removal); Fig. 15c, to an increase in the ambient temperature; Fig. 15d, to an increase in the illumination intensity; and Fig. 15e, to an increase in the voltage across the sample. Assuming that instabilities disappear near the electrothermal-breakdown temperature, the activation energy of the metastable state is estimated to be 25 meV.

Another type of oscillations was observed even without illumination. Instabilities are found at low biases following a preliminary illumination for 10 s. The monotonic relaxation of the current gave way to an oscillatory process after the current reached a certain critical value. The oscillations persisted undamped indefinitely. Unlike the preceding case, this processes cannot be understood in terms of the theory of electrothermal breakdown. Self-excited oscillations were also observed in $Pb_{1-x-y}Sn_xGe_yTe$(In) films.

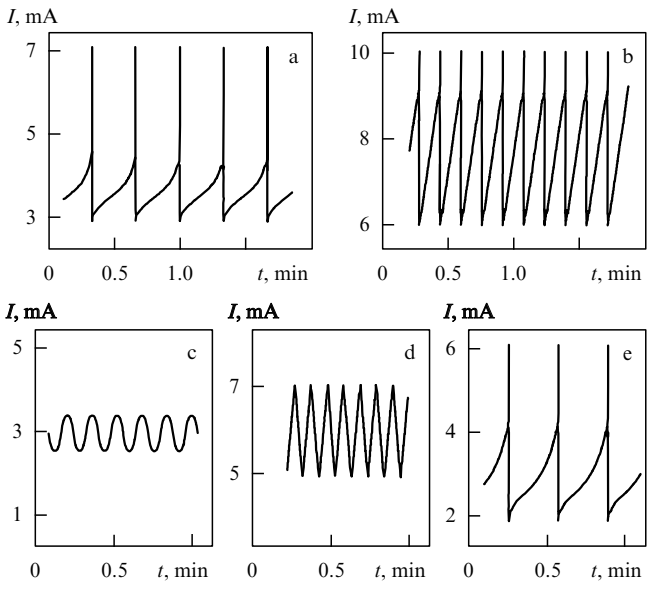

Figure 15. Thermoelectric instabilities (current oscillations) in a single crystal of PbTe(Ga) [150].

The nonequilibrium processes discussed above are another indication that the metastable impurity states arising in lead telluride-based alloys doped with indium and gallium are different from the shallow levels usually found in semiconductors. The localization and delocalization of carriers on metastable levels is characterized by a critical temperature — and hence by a potential barrier.

2.11 Effects due to a combination of external factors

When several external factors combine, new effects are observed. These effects are especially pronounced for alloys in the semi-insulating state. In this case, small changes in the relative position of energy levels (impurity levels and the edges of the allowed bands) cause a marked change in the concentration of free charge carriers. For this reason, most publications present data on indium-doped lead telluride–tin telluride solid solutions, in which the semi-insulating state is easy to realize and for which the effect of one external factor is well studied.

2.11.1 Electric and magnetic fields. A study of the $I-V$ curve of the $Pb_{1-x}Sn_xTe$(In) alloy with $x = 0.25$ at a magnetic field $\mu_0 H = 0.5$ T revealed giant negative magnetoresistance in the material. As the magnetic field is turned on, the current through the sample first increases sharply (by up to six orders of magnitude), then reaches a maximum, and finally decreases. Since the current is slow to reach its stationary value (several minutes), the shape of the curves depends on the rate at which the magnetic field is applied. The shape of the $I(H)$ curves also shows a strong dependence on the applied voltage: the maximum current increases nonlinearly with increasing U.

This effect is explained by assuming that a metastable impurity level shifts in a magnetic field [151]. If the level shifts to lower energies, the electrons localized on it go over into the conduction band, the concentration n increases — and, hence, the conductivity increases. This assumption has been confirmed in Hall-effect measurements [152]. The delocalization of electrons from traps is clearly seen even in the presence of nonequilibrium carriers excited by the background illumination of the sample.

2.11.2 Strong magnetic field and IR illumination. The experiments of Refs [152–154] used IR illumination as an additional external factor to influence the relative position of the quasi-Fermi level and the edges of the allowed bands in $Pb_{1-x}Sn_xTe$(In) alloys. The application of short and strong ($\mu_0 H > 5$ T) magnetic-field pulses led to a surprising result. Instead of an increase in the conductivity, as in weak fields, a strong magnetic field causes the localization of free photoexcited electrons and decreases the conductivity.

It is established that the increase in the sample resistivity in time is given as

$$\rho = \rho_0 + \Delta\rho\left[1 - \exp\left(-\frac{t}{\tau}\right)\right], \tag{2.4}$$

where τ depends in the following manner on T and H:

$$\tau = \tau_0\left(1 - \frac{T}{T_0}\right)\exp\frac{H}{H_0}. \tag{2.5}$$

The value $\mu_0 H_0 = 4.5$ T does not depend on the sample temperature, nor on the concentration of photoexcited carriers. The value $T_0 \approx 4-6$ K decreases with increasing carrier concentration, and at $T > T_0$ the effect disappears. At a sufficiently high concentration of photoexcited electrons, when T_0 becomes less than T, it has been shown [152] that electrons in a magnetic field are delocalized instead of being localized.

The analysis of various interpretations of the experimental data led the authors of Refs [152–154] to assume that the most likely mechanism is that in a magnetic field nonequilibrium charge carriers are localized on a metastable impurity level. This explanation, however, leaves many aspects of the problem unclear and, hence, can hardly be considered definitive. In fact, if the observed processes (delocalization in a weak magnetic field, the localization of carriers at low photoexcitation levels, and their delocalization at high photoexcitation levels in strong magnetic fields) all occur at one and the same metastable level, the structure of this level must be very unusual indeed.

3. Theoretical summary

The understanding of the anomalous behavior of impurities in semiconducting lead chalcogenide solid solutions depended on experimental data for its development. Therefore, the main basis for this development was lead telluride-based solid solutions doped with Group III elements In and Ga, i.e., the most studied system of this kind. Ideally, the theory should be able to explain within a single framework — at least qualitatively — a whole spectrum of observed phenomena: the charge states of impurity centers and chemical-potential (Fermi-level) stabilization, the long-term relaxation of electron distribution, and the optical properties and paramagnetism of Ga-doped semiconductors.

There are currently two approaches that satisfactorily explain this class of phenomena. Even though they share common features (see below), one of them may be called, somewhat loosely, a 'deformation' approach [2, 155–159]; the idea of the second may be viewed as based on the mixed-valence phenomenon in Group III dopants [127, 140, 160, 161].

Phenomenologically, both approaches assume the existence of centers with a negative correlation energy U in the system (DX-like impurity centers [75]). Such a center can have two ground states differing by two elementary charges e (the number of electrons trapped by the center being $n = 0$ and $n = 2$). The state with $n = 1$ can be observed only as excited from one of these two ground states. Precisely which of these — $n = 0$ or $n = 2$ — is realized in the system depends on the system's chemical potential μ.

The difference between the two approaches lies in the mechanism whereby the centers with negative correlation energy are thought to form. The deformation model [2] is based on the hypothesis that the electron energy of a center depends on the center position in the crystal lattice (or on the deformation of its nearest crystalline environment). In the simplest case, it is assumed that the electron energy $E_{\rm el}$ depends linearly on deformation Δ and that the total energy of the system $E_{\rm tot}$ is the sum of the electron energy of the center and the elastic deformation energy proportional to Δ^2. Thus, the total energy of the system can be written as

$$E_{\rm tot} = (E_0 - \mu)(n_\uparrow + n_\downarrow) + g(n_\uparrow + n_\downarrow)\,\Delta + \omega_0^2 \Delta^2 . \qquad (3.1)$$

Here, E_0 is the energy of the undeformed center, g is the electron–deformation-field coupling, $\omega_0^2\Delta^2$ is the deformation energy, and the $n_{\uparrow,\downarrow}$ are the electron occupancies of the center ($n_{\uparrow,\downarrow} = 0, 1$).

Eqn (3.1) ignores the Coulomb repulsion due to the double occupancy of the center ($n_\uparrow + n_\downarrow = 2$). For IV–VI semiconductors, this is fully justified by the large values of their static dielectric constants ($\varepsilon_0 \sim 10^3$). It is appropriate to note that for the same reason all impurity potentials in IV–VI semiconductors may be considered to be short-range, which, in turn, allows one to limit the consideration to the case with only one bound or resonant (neglecting spin) electron state on an impurity ($n_\uparrow + n_\downarrow = 0, 1, 2$).

Minimizing Eqn (3.1) with respect to the displacement Δ at fixed occupancy numbers (0, 1, 2) shows that for $\mu > \mu_c = E_0 - g^2/2\omega_0$ the ground state of the center involves two bound electrons ($n_\uparrow + n_\downarrow = 2$), whereas for $\mu < \mu_c = E_0 - g^2/2\omega_0$, none. When the chemical potential assumes its critical value μ_c, the total energy of the single-charge state is $E_{\rm tot} = g^2/4\omega_0$, which is more than zero. It is this value that represents the classical barrier for the impurity system to change from the two-charge to the neutral state.

Turning now to the deformation model itself, it is clear that at $\mu < \mu_c$ a defect supplies two electrons to the bands of interest (the conduction and valence bands here), and the two-electron state on the center transforms into an empty state; whereas for $\mu > \mu_c$, two electrons find themselves bound on the impurity center. At $\mu = \mu_c$, the charges redistribute themselves among the defects, leading to the stabilization of the chemical potential, until the defects outnumber the carriers (electrons or holes) introduced into the system. The requirement that Eqn (3.1) be minimized with respect to the deformation suggests that the role of the negative correlation energy U is here played by the quantity $-g^2/\omega_0$.

In Ref. [4], the role of a center with negative correlation energy was delegated to a chalcogen (Te) vacancy, which indeed is two-charge, supplying two electrons to the bands of interest. Group III impurities were believed to play a passive role as far as the electron system is concerned: a Group III atom just heals metal vacancies which supply two holes and shift chemical equilibrium in favor of the chalcogen vacancies. This seems to be a rather far-fetched assumption though, since it does not take into account the specificity of Group III elements compared to the elements of other groups.

Another drawback of the deformation model is that it is hardly compatible with the actual temperature range where long-term relaxation processes are observed. These processes stop at $T > 100$ K in lead telluride doped with gallium and at $T > 30$ K in the case of indium doping — at temperatures that are of the same order of magnitude as the frequencies of optical phonons in the IV–VI semiconductors. It is natural to identify optical phonon frequencies as the characteristic vibrational frequencies of the deformation mode. But then the barrier for thermal transitions ($W \sim g^2/4\omega_0$) turns out to be too transparent for a tunneling transition between various charge states of the defect, leaving unexplained the large (of order of hours) characteristic times for the relaxation of nonequilibrium carriers. On the other hand, if the barrier is high, it is difficult to understand why long-term relaxation processes stop at such low temperatures.

In view of the above, a more attractive model is the one exploiting the idea of the intermediate valence of Group III impurities as discussed in a review paper by Drabkin and Moĭzhes [160]. The model involving the intermediate valence

of Group III impurities in IV – VI semiconductors was further developed in a whole series of experimental and theoretical studies, references to which can be found in Volkov and Khokhlov's review talk at the 23rd International Conference on Semiconductor Physics [127] (see also Ref. [161]).

Briefly, the idea is as follows. The outer shell of the Group III elements has the configuration s^2p^1. When in compounds, however, these elements may behave as mono-, di-, or trivalent impurities, i.e., chemical bonding may involve either one electron from the p-state (configuration s^2p^1, valence $+1$), or two electrons (configuration s^1p^2, valence $+2$), or all the three electrons (configuration s^0p^3, valence $+3$); the compounds with a Group III element in a divalent state being the most unstable of these. This is quite understandable intuitively because there is only one unpaired (paramagnetic) electron left in the s shell.

In IV – VI semiconductors a Group III dopant atom (for example, gallium) replaces metal (lead), which is in the divalent state s^2p^2. If an impurity atom enters the crystal in a monovalent state, then the system will be short of one electron, i.e., a Group III atom in the s^2p^1 configuration will behave as a singly charged acceptor. In the divalent state (s^1p^2), the impurity will be neutral but paramagnetic, and in the trivalent (s^0p^3) state, a Group III atom will be a singly charged donor. In this situation, the full electronic energy of the system in a paramagnetic (s^1p^2) defect configuration can be expected to exceed the energies of the charged states (s^2p^1 and s^0p^3). This is confirmed by analytical calculations [140].

The same work showed that which of the charged configurations is realized is determined by the chemical-potential (Fermi-level) position. The point here is that in the cubic lattice of a semiconductor, the valence and conduction bands are formed by the p states of the metal and chalcogenide, the band of the s states being narrow and lying very low on the energy scale [158]. As a result, as the chemical potential moves to lower energies, it becomes easier for the electrons of the s shell to pass onto the Fermi level. Thus, it may be expected that at low Fermi levels Group III impurities should exhibit donor properties (configuration s^0p^3), whereas at high Fermi levels they should behave as acceptors (configuration s^2p^1). Clearly, at a certain critical value of the chemical potential, when the energies of both configurations are the same, a process of charge redistribution begins in the system of impurities, leading to the stabilization of the Fermi level.

The levels we have described above — that arise for various charged states of an impurity — can be considered deep because they result from the reconstruction of a defect's s shell. It has been shown, however [140], that a system of defects may also have shallow levels split from the semiconductor conduction-band bottom by a short-range attractive potential due to a Group III atom in the s^0p^3 (donor) configuration. This is because the s shell of the defect in this configuration is empty, thus enhancing the attractive force of the impurity's core on the p electron. If the short-range potential is strong enough, it may create a shallow bound state close to the conduction-band bottom.

The hydrogen-like levels of IV – VI semiconductors are hardly worth discussing because of the huge static dielectric constant ($\varepsilon_0 \sim 10^3$) and low (about $10^{-2}m_0$) effective mass — which reduces the effective Ry^* by a factor of 10^7 as compared to the true Ry.

If the short-range (pointlike) potential of an individual impurity is not sufficient to produce a bound state, a system of such impurities can do the job [162]; this leads to the stabilization of the Fermi level within the conduction band in IV – VI semiconductors doped with Group III elements. Otherwise, the appearance, under the band bottom, of a sufficiently deep bound hydrogenic state similar to those in classical semiconductors (Ge, Si, GaAs, etc.) would lead to the localization of all the electrons coming to the conduction band from the impurity s shells. This may occur on the so-called DX-centers, whose nature may be similar to that of the centers we discuss here. Therefore, centers created by Group III impurities in IV – VI semiconductors may be called DX-like centers. The presence of shallow bound states in the short-range potential due to Group III impurities in the configuration s^0p^3 may help in explaining a sharp absorption peak in the immediate neighborhood of the intrinsic absorption edge in doped IV – VI semiconductors [136, 161] and in explaining the dynamic paramagnetic anomaly in PbTe(Ga) [147].

It is appropriate here to see how the mixed-valence model explains the long-term relaxation of nonequilibrium carriers in IV – VI semiconductors doped with Group III elements. The mechanism of long-term processes is obvious by itself. Both the transfer of charge carriers from the state s^2p^1 to the state s^0p^3 and the inverse recombination process should necessarily pass through the intermediate state s^1p^2 because any boson (photon, phonon) field can change the state of only one fermion in a single event. This statement is exact within the Hartree – Fock approximation, in which the wave function of a fermion system has the form of a determinant.

In principle, systems with interaction may involve processes whose amplitude is described by the following skeletal diagram:

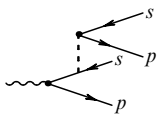

Here, the wavy line denotes the D function of a photon (phonon), the dashed line stands for the electron – electron Coulomb interaction, and the solid lines correspond to the electron propagation functions.

The diagram describes the transition of two electrons from the s to the p state, when one of the electrons is 'shaken' by the external field and the resulting Coulomb field excites the second electron. Usually, such processes are strongly suppressed or even forbidden for reasons of symmetry [163]. As a result, because the energy needed to excite an electron to the neutral (s^1p^2) state of a Group III atom exceeds the energies of the charged configurations, an energy barrier for generation and recombination processes appears, which slows down these processes dramatically at low temperatures.

It is important to note that the above models are inadequate for another Group III element, thallium. The behavior of thallium in IV – VI semiconductors is analyzed in detail in a review paper by Nemov and Ravich [9]. Experimental data are interpreted there by introducing self-compensation and considering a deep resonance level with a high density of states near the top of the second valence subband. The question of the charged states of gallium atoms in a telluride matrix remains open.

Cr, Gd, and Yb are also mixed-valence dopants and also remain virtually unexplored theoretically. The presence of a magnetic moment in transition-metal impurity atoms makes

it possible (by directly measuring the magnetic moment) to establish their charged states and to show that, unlike In and Ga, their valence changes by unity. In recent years, a large amount of experimental data on materials of interest here has been gathered, and it is hoped that the development of a microscopic theory will stimulate further experimental research in the field.

4. Applied aspects

Most of the photodetecting systems currently operating in the far infrared range (20 – 200 μm) are based on 'classical' semiconductor materials — germanium or silicon — doped with shallow impurities [164]. The largest wavelength for quantum detectors of radiation — one corresponding to the red edge of the photoeffect — is currently $\lambda_{red} \approx 220$ μm [165] and is observed in uniaxially deformed Ge(Ga).

The primary advantage of germanium and silicon as compared to other semiconductors is the highly sophisticated preparation technology yielding high quality crystals with extremely small amounts of uncontrolled impurities and growth defects. In spite of the small excitation energies of impurity levels, the resistivity of photodetectors at low temperatures (1.5 – 4.2 K, a temperature range securing high sensitivity in the far infrared) is typically very high, about 10^5 Ω cm.

There is a down side to all this, however, namely, low radiation hardness. Hard radiation falling on a very pure semiconductor easily produces enough defects to exceed the residual concentration of impurities and defects, thus degrading the performance of the entire photodetecting system of which the semiconductor is a part. There is also another problem to consider. If heavily doped germanium or silicon are used, then, because of the relatively large Bohr radius of shallow impurity states, an insulator – metal transition takes place, giving rise to impurity-band conduction which shunts the photoconductivity signal. In a lightly doped material, for which impurity centers may be considered isolated, absorption at wavelengths corresponding to impurity – band transitions will be small, so that to achieve high quantum efficiency, thick (up to 1 cm) samples are required.

The above drawbacks are overcome in part by using blocked impurity band (BIB) structures [166, 167], which are obtained by depositing a layer of undoped semiconductor between a heavily doped region and the electrode.

The unique properties of narrow-band IV – VI materials doped with Group III elements indium and gallium offer a very promising alternative for designing highly sensitive photodetectors for the far infrared range. The IV – VI semiconductors are one of the basic materials of modern IR optoelectronics. The narrow forbidden band (which may vary smoothly with the composition), the direct gap, high radiation yield, and other features make this semiconductor family very attractive for applications in IR technology.

Photodetectors on the basis of PbS, developed as long ago as in the 1940s, were among the first sensitive quantum detectors of midinfrared radiation. The IV – VI semiconductors are widely used to produce lasers and light-emitting diodes operating in the middle and far infrared portions of the spectrum [168]. Significant progress has been made in the development of large focal photodiode arrays based on IV – VI semiconductors and adapted to read-out silicon electronics by means of thin buffer fluoride layers [169].

By the mid-1980s, traditional IV – VI IR detectors started, mainly because of their high defect content, to give way the position to much more advanced detectors based on $Hg_{1-x}Cd_xTe$. In about the same period, fundamental studies of the impurity states in lead telluride-based alloys doped with Group III elements enabled the development of fundamentally novel mid- and far-infrared photodetectors.

Intensive applied research stimulated by fundamental studies is currently showing much promise because the performance of far-infrared detectors has been found to be comparable to or better (sometimes by orders of magnitude) than that of the state-of-the-art Ge- or Si-based analogues. The following sections discuss the physical principles of photodetecting systems using doped lead telluride-based alloys, describe the advantages of these systems over traditional ones, and make a direct comparison between these systems and their best traditional counterparts.

4.1 Electrical and physical homogeneity and the radiation hardness

From the viewpoint of IR-detector design, the most promising compounds of those listed in the table in Section 2.2.2 are PbTe(Ga) and indium-doped PbTe – SnTe solid solutions. Compared to the others, they are the most completely studied, and the technology for reproducibly manufacturing high-quality samples has been developed for them in most detail. There are, however, also fundamental reasons for this choice. Unlike most other impurities, indium and gallium leave the energy spectrum of the host alloy unchanged, thus enhancing the reproducibility of detector parameters and reducing band-edge potential fluctuations due to the inhomogeneous impurity distribution.

Second, it is the PbTe – SnTe solutions where impurity levels change their position most smoothly with the composition, thus allowing one to achieve more or less effortlessly the energy spectrum parameters required for the photodetector material. In other solid solutions, e.g., PbTe – MnTe, the position of the stabilized Fermi level changes more rapidly with composition, so that the electrical and physical parameters are much less homogeneous even though a semi-insulating state can be realized.

Indium and gallium in lead telluride-based alloys secure Fermi level stabilization due to the valence instability of the $In^+ - In^{3+}$ type. Hence, in the materials under study, indium and gallium can exhibit electroactivity of both *n* and *p* types, enabling one to effectively screen out uncontrolled charged impurities and defects of both signs by spatially redistributing the charged states of a Group III impurity. Thus, PbTe(In) turns out to be more homogeneous electrically than nominally undoped PbTe.

An important consequence of Fermi-level stabilization is that the energy-spectrum parameters of PbTe(In) and PbTe(Ga) are perfectly reproducible irrespective of the way the sample is prepared. This determines the high yield and low production cost of the materials under study.

The high radiation hardness is yet another advantage of $Pb_{1-x}Sn_xTe$(In)-based photodetectors. This property is a consequence of the high density (of order 10^{20} cm^{-3}) of Fermi-level-stabilizing impurities. As long as the density of defects caused by hard radiation is below the impurity concentration, the Fermi level remains stabilized and the photoelectric properties of the sample remain unchanged as well. Irradiation by fast electrons with an energy of 5 keV and a dose of up to $10^{17} - 10^{18}$ cm^{-2} causes no changes in the

sample response [170]. This dose is at least four orders of magnitude greater than the limiting dose for other sensitive IR detectors based on Ge- and Si-doped $Hg_{1-x}Cd_xTe$.

It should be particularly noted that the realization of a semi-insulating state in a doped lead telluride-based alloy gives rise to a situation, highly unusual for semiconductor physics, in which a heavily doped narrow-band semiconductor with a large number of growth defects behaves (from the viewpoint of electrical properties) as an almost ideal semiconductor which has a virtually zero low-temperature carrier concentration and is highly homogeneous electrically. This makes such materials very attractive for IR detectors.

4.2 Quenching of persistent photoconductivity

One of the important performance parameters of a photodetecting device is the lifetime of photoexcited charge carriers τ. The output signal of an individual photodetector is generally proportional to τ. At the same time, τ should not exceed the response time τ_r required of the detector because otherwise the output signal will not correspond to the incident radiation intensity in a unique way.

For $Pb_{1-x}Sn_xTe$(In) and PbTe(Ga) alloys, the lifetime τ can be varied over a very wide range (from 10^{-3} to 10^5 s) by varying the composition, impurity concentration, and temperature. For $Pb_{1-x}Sn_xTe$(In), the characteristic time of the slow component of the relaxation process (it is the time that determines the value of τ) varies from 10^5 s at $4.2\ \text{K} < T < 10\ \text{K}$ to 10^{-2} s at $T = 20$ K. For PbTe(Ga), $\tau > 10^5$ s for $4.2\ \text{K} < T < 45\ \text{K}$, and as the temperature is increased, τ drops to 10^{-3} s at $T = 77$ K.

It follows, then, that the operating temperature of a photodetector can be chosen based on the required speed of response. Examples of detectors on the basis of $Pb_{1-x}Sn_xTe$(In) are known for which limitation by background radiation is realized at an operating temperature $T = 25$ K [134].

If the temperature of the sample is such that $\tau > \tau_r$, then the output signal no longer corresponds to the incident intensity and is in a sense 'integrated' by the photodetector. Generally speaking, the integration of the light flux incident on a photodetector is one of the major ways of improving the signal-to-noise ratio. Such integration is usually realized either by creating potential wells in the detector by using the field effect, or by integrating the signal in outer electrical circuits. Both possibilities are difficult to realize, however, especially if applications to photodetecting arrays are concerned.

The relatively limited dynamic range is another drawback of these methods. The persistent-photoconductivity effect offers a unique opportunity to integrate the incident light flux 'internally,' when photoexcited free carriers are accumulated not in artificially created structures but — owing to the physics of the process — directly in the sample itself.

At the same time, the regime of internal integration of a signal is only possible if the sample's original darkness state can be restored, i.e., if persistent photoconductivity can be rapidly quenched. There are several ways of doing this.

First, photoexcited free carriers can be localized on an impurity ground state by simply heating the sample to a temperature $T > T_c$ and then cooling it in darkness [77]. This process, however, is too slow to be useful in real photodetectors.

Persistent photoconductivity can also be quenched by delivering an electric field pulse to the sample contacts. In this case the system returns to the initial semi-insulating state as a result of an electrothermal breakdown [103]. The quenching of persistent photoconductivity in this situation is complete only in the photomemory regime, i.e., when the IR radiation source is off. Otherwise, the quenching is unstable and incomplete. Besides, the minimum value of conductivity after the quenching pulse is greater than the original darkness value and, in addition, varies from pulse to pulse. Moreover, the periodic application of strong electric-field pulses to the sample contacts leads to a gradual and irreversible degradation of the photoresponse and, ultimately, to its full disappearance [103].

The partial quenching of persistent photoconductivity by short-wavelength laser pulses was observed in Refs [93–95]. The effect was described in terms of negative photoconductivity (see Section 2.7). From the application viewpoint, it is important that the 'infrared' quenching is very fast but incomplete. Moreover, similar experiments on bulk crystals of $Pb_{1-x}Sn_xTe$(In) of the same composition failed to show negative photoconductivity [171].

Yet another possibility is to make use of strong field domains that are formed in the material. This effect was observed in $Pb_{1-x}Sn_xTe$(In) alloys, in which the Fermi level is stabilized in the conduction band. A high-field domain is formed in a certain region of the sample after a strong and short (of order 10^{-7} s) pulse of electric field has been applied. It is interesting that for a sample initially in a semi-insulating state, applying an electric field returns the system to its equilibrium state. By contrast, in a sample whose equilibrium state is 'metallic,' the electric field creates a nonequilibrium situation in which free electrons are trapped by an impurity quasi-local ground state resonant with the conduction band.

In the last case, the concentration of free carriers in a domain is much lower than the equilibrium low-temperature value. The electrons trapped by impurity centers slowly go over to the conduction band at $T < T_c$. The characteristic time for such transitions is comparable to that for the relaxation of persistent photoconductivity. Since the size of a domain is usually much smaller than that of a bulk crystal sample, a semi-insulating high-field domain is formed only in a certain region of the sample. The size of this region varies somewhat from pulse to pulse, increasing the noise level in the system.

In films, it is possible to concentrate the electric field artificially in a smaller-than-domain region of the sample. The region of domain formation thus proves to be limited geometrically, with the consequence that the resistance of the film is restored after the field pulses. Applying IR illumination greatly increases the rate at which the conductivity relaxes to its equilibrium value.

Thus, when electric field pulses are applied periodically, the output signal has a saw-toothed shape, its amplitude being proportional to the radiation flux incident on the sample. In an experiment described in Ref. [172], radiation arrived at the sample from a thermal source which was first heated from 4.2 to 20 K and then cooled down. A measurable photoconductivity signal appeared at the source temperature above 15 K.

The purely electric quenching mechanism described above has a major drawback, however: the sample resistance is relatively low after quenching. (The electric field is concentrated in a relatively small region of the sample, so the injection current — and hence the effective conductivity —

are very high.) To increase the initial sample resistance, it is necessary to increase the size of the high-resistance region.

The quenching of persistent photoconductivity by microwave pulses is free from this drawback. In this technique the sample is placed in a microwave resonator or, alternatively, microwave pulses are sent to the sample's contacts directly. Experiments described in Refs [173, 174] were made on $Pb_{0.75}Sn_{0.25}Te$(In) samples with the Fermi level stabilized within the forbidden band. The pulse frequency was about 250 MHz, the pulse intensity up to 0.9 W, and the pulse duration from 10 μs. Sample resistance after each microwave pulse did not differ from the original 'darkness' value.

In all likelihood, the electric field distribution is more uniform with microwave quenching than with the electric field pulse technique, in which practically all voltage drops across the high-resistance domain and the rest of the sample remain all but unaffected by the electric field. This is the reason why a semi-insulating state extends throughout the entire sample in the case of microwave quenching.

Note also that electric field pulses produce a non-equilibrium state, which relaxes to the equilibrium 'metallic' state even in the absence of IR illumination, whereas microwave pulses, on the contrary, restore the sample to the semi-insulating state. This is another advantage of using the microwave technique to quench persistent photoconductivity.

The microwave quenching mechanism is due to the direct interaction of microwave radiation with photoexcited electrons. In fact, the crystal lattice remains unheated after the microwave pulse is over [174]. One possible explanation is that the electron gas is heated by microwave pulses directly. In this case, one would expect that the efficiency of quenching will be independent of the microwave frequency, although there is some evidence to the contrary.

In Ref. [175], a $Pb_{0.75}Sn_{0.25}Te$(In) sample at 4.2 K was simultaneously connected to two electric circuits, one of which was used to measure the dc conductivity and the other, for the microwave pumping of the sample. The frequency of the microwave generator varied from zero to 500 MHz. The intensity of the applied microwave pulse was 50 mW, much lower that the minimum microwave intensity (900 W) required for quenching. The characteristic measured was the dependence of the sample's dc conductivity σ on the microwave pumping frequency ω.

In the initial 'darkness' state, no conduction was observed over the entire frequency range (Fig. 16). As IR exposure was increased, a sharp peak in the $\sigma(\omega)$ dependence appeared against a growing conductivity background. When the IR source was turned off, the conductivity slowly relaxed to the darkness value; however, the relaxation rate outside of the peak greatly exceeded that near the peak on the (microwave) frequency scale. This enabled the researchers to achieve a virtually nonconducting state at all pumping frequencies (including $\omega = 0$), except for the peak region.

The frequency position of the peak was independent of the applied electric field but varied strongly with magnetic field. The sensitivity of the conductivity to repeated exposures to IR illumination during microwave pumping at the peak frequency was much higher than for the initial 'darkness' state. Although nothing like a certain interpretation of this effect is given in Ref. [175], the impression is that it is due to the microwave stimulation of quantum efficiency (see Section 4.3). Both effects were observed in one and the same microwave region. It is very likely that relaxation onto metastable impurity states is responsible for both effects.

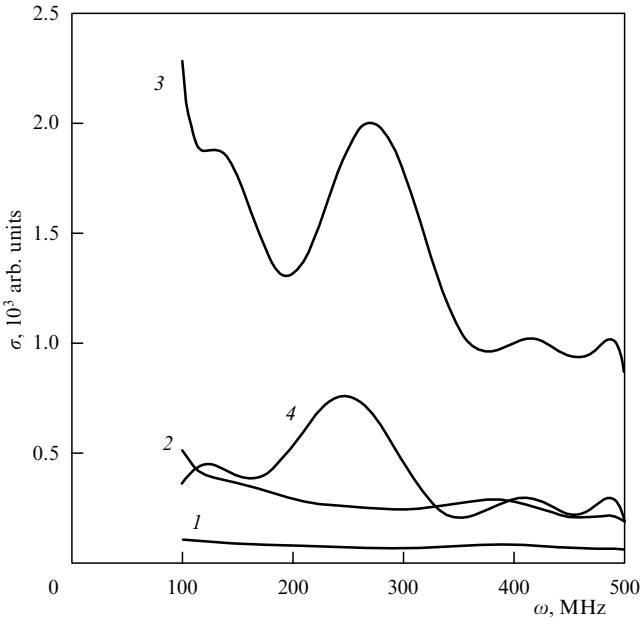

Figure 16. Conductivity $\sigma(\omega)$ of the $Pb_{0.75}Sn_{0.25}Te$(In) sample versus microwave pumping frequency for increasing IR exposure times (curves *1–3*) and after relaxation to a metastable state (curve *4*) [175].

4.3 Microwave stimulation of quantum efficiency

Applying a microwave pulse not only leads to the quenching of persistent photoconductivity but also affects the kinetics of photoresponse following the pulse. As shown in Ref. [174], the quantum efficiency of a photodetector increases to $\eta \sim 10^2$ if persistent photoconductivity is quenched by a microwave pulse with the duration and intensity at the minimum required for quenching. Outside the quenching regime, $\eta \sim 1$. It is important to note that an enhanced quantum efficiency is observed only for the conductivity range $0 < \sigma < \sigma_{th}$; for $\sigma > \sigma_{th}$, photoconductivity grows at the same rate as outside of the regime of quantum-efficiency stimulation.

At a qualitative level, the explanation of this effect may be as follows [174]. When a short-duration microwave pulse of a sufficiently low intensity is applied, photoexcited electrons pass onto a metastable impurity state E_1 rather than on the ground state. Since the barriers that separate these metastable states both from the band states and from local ground states are relatively low ($W \approx 1$ meV [103]), a longer or a more intense microwave pulse bring all the photoexcited electrons into the ground state E_2.

Thus, the application of a sufficiently weak, short microwave pulse increases the population of metastable impurity states. Since these local states are much less localized than the ground states [176], strong-coupling clusters can be formed by some of the impurity centers E_1. Then, the photoexcitation of an electron from one center in the cluster initiates the avalanche depletion of all the remaining centers, thus increasing the quantum efficiency.

4.4 Spectral sensitivity

As discussed above, the photoconductivity relaxation process has two components, one relatively fast and the other slow. At low temperatures T, the slow component transforms into photomemory, but as T approaches T_c, the temperature at which delayed photoconductivity appears, the characteristic

time of slow relaxation becomes sufficiently short, allowing the use of standard spectroscopic equipment to measure photoconductivity spectra.

The common feature of the spectra obtained is a sharp peak at an energy corresponding to the width of the energy gap (see Fig. 14). From the viewpoint of application, it is important that this energy can vary with the temperature and composition of the alloy. In particular, for PbTe(Ga) alloys, the wavelength corresponding to the peak can be varied from 3.0 to 5.5 μm.

Direct experiments performed in Ref. [177] showed that $Pb_{1-x}Sn_xTe$(In) alloys exhibit a very strong response in the subgap region. The IR sensor used was an epitaxial film of $Pb_{0.75}Sn_{0.25}Te$(In) cooled to liquid-helium temperatures. The background radiation was to a considerable extent, but not completely, screened. The source of radiation was a blackbody at a temperature of 300 or 77 K. The radiation passed through a system of cooled filters, which cut a narrow stripe at a wavelength of either 89 or 115 μm depending on the last-to-pass liquid-helium-cooled filter. At both wavelengths, a considerable photoresponse was observed.

It is important to note that the energy of the quantum that corresponds to the experimentally used values of λ is much less than the thermal energy for activating the impurity ground state. This means that the electrons dominating the effect are localized in a metastable impurity state rather than in the ground state. Filling these states by using microwave pulses (quantum efficiency stimulation), electron injection from the contacts, and background IR illumination leads to a 'red' shift λ_{red} relative to the nonexcited 'darkness' state. The value of λ_{red} for this case has not yet been determined, but there is reason to believe that it can be very large, so that the photodetectors of interest here may be sensitive over the entire submillimeter range.

This conclusion can be drawn from measurements on PbTe(Ga) in the far-infrared range. Assuming similarity between DX-like centers in $Pb_{1-x}Sn_xTe$(In) and PbTe(Ga), one would expect that the photoconductivity spectra of these materials are also similar, of course, to within the difference between the characteristic energies of their respective spectra.

The far-infrared spectrum of the fast photoconductivity of PbTe(Ga) was studied in Ref. [178]. The spectrum was found to consist of a narrow line at a frequency $\omega = 155$ cm^{-1} and its repetitions at the integer multiples of this frequency (curve *1* in Fig. 17). In most cases, this line is resolved only in a narrow temperature range (57 – 63 K) with a maximum at 60 K. The amplitude of the peak is maximum immediately after the sample is cooled to 60 K. If the temperature is fixed, the photoresponse gradually decreases to virtually disappear in about 40 min. As the temperature is varied at least by 10 K to either side, the fundamental photoconductivity line reappears at 155 cm^{-1}.

As the sample is cooled to 60 K with an additional relatively short-wavelength illumination in the region of fundamental absorption, the far-infrared spectrum first looks similar. The 155-cm^{-1} line quite rapidly disappears, but after that a broad large-amplitude photoresponse band appears (curve *2* in Fig. 17). The red edge of the photoeffect for this band is at a wavelength in excess of 500 μm. As long as the short-wavelength illumination is on, the picture remains stable. When it is turned off, this far-infrared photoresponse disappears.

If the analogy between PbTe(Ga) and $Pb_{1-x}Sn_xTe$(In) is valid, then the photoconductivity spectra of the former

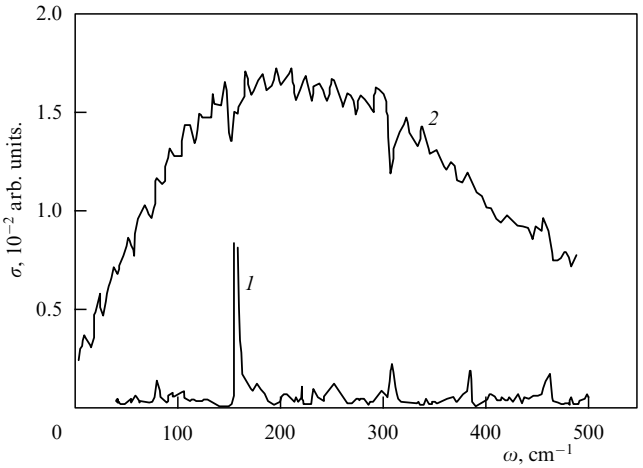

Figure 17. Photoconduction spectra of PbTe(Ga) in the far-infrared range recorded immediately after cooling the sample to 60 K (curve *1*) and under additional short-wavelength illumination (curve *2*) [178].

should have the same features as those of the latter, but their spectral positions should be shifted toward longer wavelengths, and measurements should be made at lower temperatures. Also, the value of λ_{red} may considerably exceed the maximum value $\lambda_{red} = 220$ μm observed in current photodetectors.

4.5 Radiometric parameters

In Ref. [179], a $Pb_{1-x}Sn_xTe$(In)-based laboratory radiometer is described, whose operation involves a periodic buildup of the signal followed by a rapid quenching of persistent photoconductivity by a microwave pulse. As a source of IR illumination, a blackbody was used. The design insured that the sample was completely screened from the background radiation. The blackbody and the sample were placed in a liquid-helium-cooled vacuum chamber. Between the blackbody and the sample, an electromechanical radiation-flux interrupter, a calibrated stop aperture, and a grid filter were placed.

All elements of the device were at liquid-helium temperature. The temperature of the blackbody was varied from 4.2 to 300 K by moving the blackbody relative to the liquid-helium level. The stop aperture limited the field of view of the sample to the blackbody cavity irrespective of the cavity position. This method of changing the blackbody temperature was advantageous in that all parts of the radiometer, including the blackbody, were in thermodynamic equilibrium with their environment. If the position of the blackbody were fixed and its temperature changed by, say, a heater, it could not be guaranteed that the stop aperture and filter will not be heated.

These precautions are very important because the wavelength of the red edge of the photoeffect is very long in this photodetector, and even a weak heating of the stop aperture or the filter may affect the photoresponse. A grid filter effectively cuts off blackbody radiation at wavelengths $\lambda > 18$ μm. Because the value of λ_{red} is much higher than that, the flux of effective quanta to the detector can be calculated quite accurately for any blackbody temperature.

The read-out electronics used in the study of Ref. [179] was not particularly sensitive; for example, currents below 10^{-7} A could not be detected. Nevertheless, it proved possible to detect a photon flux $N = 2 \times 10^4$ s^{-1}, corresponding to a

noise-equivalent power (NEP) of 2×10^{-16} W for a photodetector area of 0.3×0.2 mm^2 and a frequency of measurement of 3 Hz. The detector's current responsivity in this regime turned out to be giant, $S_I \sim 10^9$ A W^{-1}, but the low sensitivity of the measuring electronics made it impossible to obtain lower NEP values. The detector also worked well at higher — up to 10 kHz — frequencies of measurement.

In Ref. [177], the performance of a $Pb_{1-x}Sn_xTe$(In) photodetector is compared with that of the state-of-the-art samples of single Si(Sb) and Ge(Ga) photodetectors. The detectors were mounted on a holder attached to the bottom of a helium bath on the vacuum-vessel side. To minimize the background radiation, a screen was attached to the bottom of the bath. There was also another screen, which was held at liquid-nitrogen temperature. At the room-temperature level, the vacuum vessel was separated from the atmosphere by an inlet opening. The radiation source used was a blackbody at a temperature of 300 or 77 K.

In its way to the sample, the radiation flux from the blackbody passed through a series of filters, including an inlet opening at 300 K, a filter on the nitrogen screen, another one on the helium screen, and finally a filter on a rotating cassette inside the helium screen. The aperture on the helium screen limited the field of view to the inlet opening. A sample of $Pb_{1-x}Sn_xTe$(In) was transformed into the ground ('darkness') state by first heating it to $T_c \approx 25$ K and then cooling, the entire cycle lasting 3 to 5 min. The darkness $I-V$ curve (curve D in Fig. 18a) of the $Pb_{0.75}Sn_{0.25}Te$(In) film 1.8 μm in thickness and 1.5×0.2 mm^2 in area was measured with background radiation fully screened out, when instead of a filter, a metallic plate was placed on the helium screen. The rhombi in Fig. 18b correspond to a similar 'darkness' curve for a Si(Sb) BIB structure.

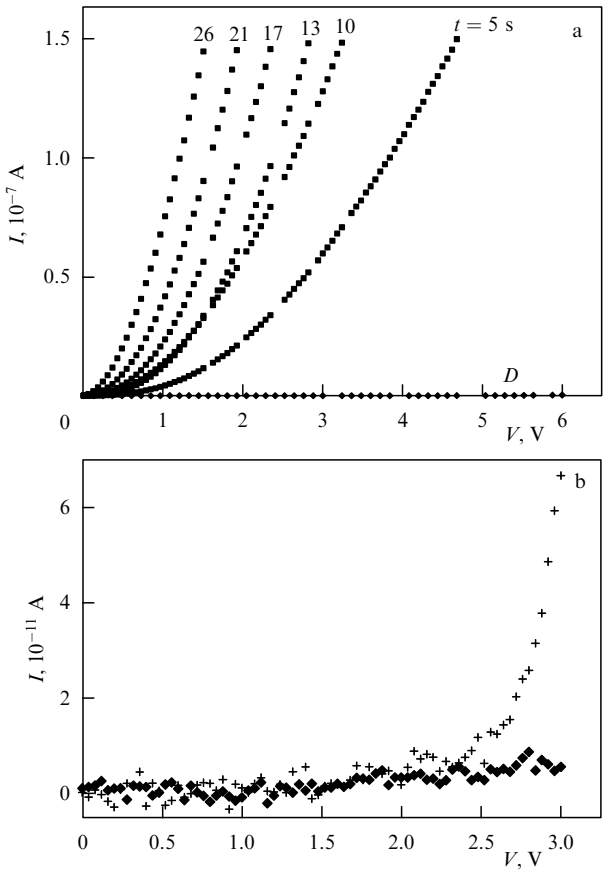

Figure 18. (a) I – V curve of a $Pb_{1-x}Sn_xTe$(In) film, measured under the conditions of darkness (curve D), and its evolution under the influence of 14-μm 'light leakage'. Numbers on the curves correspond to the time (in minutes) after the sample is cooled to 4.4 K. (b) I – V curve of a Si(Sb) BIB-structure, recorded under the conditions of darkness (rhombi) and under the influence of 'light leakage' [177].

The standard experimental procedure used for detectors based on doped silicon and germanium is as follows. First, the $I-V$ curve is measured under conditions in which most of the flux to the sample is blocked by a metallic plate placed on a cassette mounted inside the helium screen, the filter on the cassette being off the main IR beam. Then the cassette is rotated in such a way that most of the flux arrives at the sample through a filter. The characteristic time for this manipulation is several seconds. After that, the $I-V$ curves at 300 and 77 K are measured. Since the transmission spectra of all the filters are known, both the photon flux to the sample and the incident intensity can be calculated. Knowing the detector's photoconductivity for each flux value, one obtains the basic parameters of the detectors, such as quantum efficiency, current responsivity, etc., for each specified value of voltage across the sample.

Repeating the same procedure for a film of $Pb_{0.75}Sn_{0.25}Te$(In) and a series of 14-μm filters led to the overloading of the amplifier (the current through the sample > 0.25 μA) even at 40 mV, the minimum allowed voltage across the sample, for a period of time comparable to the characteristic rotation time of the cassette. Furthermore, even when most of the flux was blocked by the metallic plate, the current increased with time. This implies that there is a 'light leakage' through the gap between the cassette and the helium screen due to the multiple reflection of the incident radiation. It is to be noted that the walls of the helium screen were covered with black paper with a very low reflection coefficient. Figure 18a shows the $I-V$ curves recorded at various time intervals after the film was cooled to the liquid-helium temperature.

The 'light leakage' was also detected by a Si(Sb) BIB structure. The photocurrent associated with this leakage was as low as 10^{-12} A for the maximum voltage used, 2.5 V (crosses in Fig. 18b), whereas the photocurrent in the $Pb_{0.75}Sn_{0.25}Te$(In) film measured immediately on cooling to helium temperature was on the order of 10^{-7} A at the same voltage (Fig. 18a). Applying the currently available calibration to the BIB structure allowed an estimate of the 'light leakage' photon flux (of order 10^4 s^{-1}), yielding $\eta \sim 1$ for the $Pb_{1-x}Sn_xTe$(In) detector's quantum efficiency in this spectral region. To obtain a more accurate value, a more accurate signal buildup time is needed.

Similar measurements were made for two other series of filters, transmitting the wavelengths of 89 and 115 μm. In both cases the 'light leakage' is again present, but its intensity is much lower than for the 14-μm series. The rate of photoresponse buildup is also much lower. For voltages of 2 and 4 V, the amplifier is overloaded within a few seconds after the main light flux is delivered to the sample, whereas for 40 mV, which is the operating voltage for germanium-doped BIB structures in the same spectral region, this takes several tens of seconds to occur (Fig. 19).

This gives more accurate estimates for the quantum efficiency: $\eta \approx 0.5\,\%$ for $\lambda = 89$ μm and $\eta \approx 1\%$ for $\lambda = 115$ μm. The estimates are reasonable, because the spectral range of interest corresponds to the reststrahlen

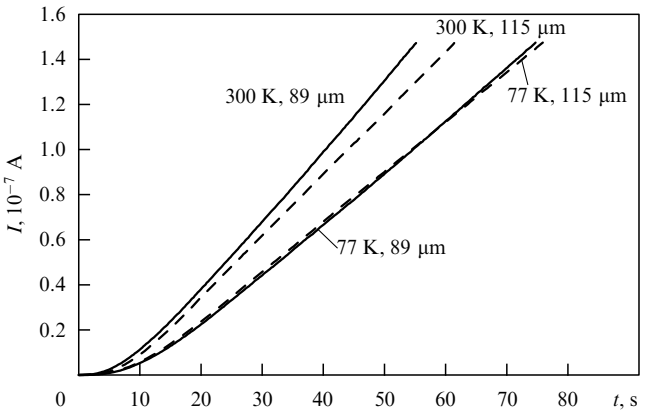

Figure 19. Photoconductivity kinetics in a $Pb_{1-x}Sn_xTe(In)$ film exposed to blackbody radiation filtered at 89 and 115 μm. The numbers on the curves are the blackbody temperature and wavelength, $T = 4.2$ K. Illumination starts at a time $t = 0$ (to within 3–4 s). Voltage across the sample is 40 mV [177].

band for lead telluride-based alloys, and up to 90% of the incident radiation is reflected by the lattice. Antireflection surfaces and microwave-stimulated operation should increase quantum efficiency. The current responsivity of the detector at 40 mV is 10^3 A W^{-1} for a buildup time of 1 s. The current responsivity of a germanium-doped detector does not exceed 3.5 A W^{-1} in the same spectral range.

It is important to note that the electron mobility in the film used in Ref. [177] was very low, only 1200 cm^2 V^{-1} s^{-1} at $T = 4.2$ K, which is two orders of magnitude lower than in good-quality bulk samples. However, attempts in Ref. [177] to determine the photoresponse characteristics of a bulk sample proved unsuccessful: when cooled in complete darkness, the sample became semi-insulating at low temperatures. For the setup with a metallic plate covering the helium screen [177], the same sample had a resistance of at least less than 2 kΩ when 'annealed' to 25 K and then cooled to 4.2 K.

This result can be attributed either to a very small 'light leakage, which, given the sample's high sensitivity, is enough to affect it even with the helium screen covered; or to a very long-wavelength residual radiation from the screen itself. In any case, the residual radiation flux estimated using a Ge(Ga) BIB structure was at least less than a few tens of photons per second. To determine the detector performance, the microwave quenching of persistent photoconductivity should be realized.

4.6 'Continuous' IR array. Readout techniques

The specific properties of impurity states in $Pb_{1-x}Sn_xTe(In)$ permit creating a unique object, a 'continuous' focal array operating in the far infrared range. This has to do with that fact that for IR radiation acting locally photoexcitation is also local, i.e., persistent photoconductivity is observed only in the illuminated region of the sample, and photoexcited electrons do not diffuse to the nonilluminated regions [180]. The same situation occurs in the photomemory regime, i.e., after the source of IR illumination is turned off. The characteristic propagation time for photoexcitation exceeds 10^4 s at $T = 4.2$ K. From theoretical estimates, the length scale of the free electron concentration variation is about 10 μm. Experimentally, this length is found to be at least less than 100 μm [180]. The observed effect is due to the fact that, on the one hand, photoexcited free electrons cannot go too far from the generating impurity centers (the reason being the electrostatic attraction); on the other hand, they cannot recombine because of the barrier between the localized and band states.

Thus, the spatial distribution of the IR radiation dose (which is the product of radiation intensity and exposure time) is uniquely reflected in the spatial distribution of the concentration of long-lived nonequilibrium charge carriers. In other words, one can construct a 'continuous' focal array such that the signal is integrated in each of its effective elements. In such an array, geometric noise due to inhomogeneous parameters of individual elements should be minimum due to the high spatial homogeneity of $Pb_{1-x}Sn_xTe(In)$ alloys with a stabilized Fermi level.

Information readout from the 'continuous' array is a separate problem. There are a number of alternative ideas concerning readout. In the contact read-out approach, the sample is provided with two sets of mutually perpendicular contacts insulated from each other at each site of the resulting grid. The resistance of the sample in the vicinity of each site can be obtained by multiplexing the series of contacts in a special way; as a result, the distribution of IR radiation dose over the sample surface can be restored. This approach requires $2n$ independent contacts, n^2 being the number of grid sites. At large values of n, additional heat transfer to the sample can be a problem, and some difficulties in contact multiplexing may arise.

A second technique is reading by an electron beam in a contactless fashion. In this technique, however, a variety of problems, both engineering and fundamental, arise. First, a high-vacuum system operating at liquid-helium temperatures is difficult to realize. Second, the sample should be screened from the direct IR radiation from the heated cathode of the electron-beam tube. Finally, it is not quite clear how the electrons arriving at the sample influence the persistent photoconductivity effect.

A third approach, proposed in Ref. [179], appears to be the most promising. Consider a thin enough sample of $Pb_{1-x}Sn_xTe(In)$ having a semi-transparent electrode deposited on one of its faces (Fig. 20). The IR flux under study reaches the sample from the left. Deposited on the opposite face of the sample are a buffer (lattice-matching) layer of BaF_2, a thin layer of silicon or other relatively wide-bandgap semiconductor material, and then a second semitransparent layer.

If this structure is illuminated by a long-wavelength laser locally from the right, a highly conducting region can be created in the wideband semiconductor in the laser spot. If one now applies a voltage across the electrodes, then the current in the system will be determined by the conductivity of the $Pb_{1-x}Sn_xTe(In)$ layer in the spot region because the effective thickness of the semi-insulating wideband semiconductor is much less there.

Using the readout idea of Fig. 20 can reduce the darkness current substantially compared to conductivity measurements on $Pb_{1-x}Sn_xTe(In)$. From the viewpoint of darkness current reduction, this idea is reminiscent of the operating principle of BIB structures using silicon or germanium doping. If the relaxation rate in the wideband semiconductor is sufficiently high, then the distribution of free carrier concentration in $Pb_{1-x}Sn_xTe(In)$ can be reconstructed by simply scanning a laser beam across the sample surface and measuring the corresponding current in the structure.

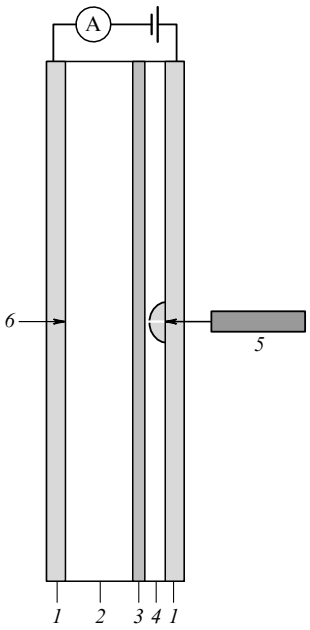

Figure 20. Device for information readout from a 'continuous' focal array on the basis of $Pb_{1-x}Sn_xTe(In)$ [37]: *1*, semitransparent electrode; *2*, active layer of $Pb_{1-x}Sn_xTe(In)$; *3*, buffer layer of BaF_2; *4*, layer of silicon (or another relatively wide-band, semiconductor); *5*, short-wavelength laser; and *6*, IR radiation flux under study.

Unfortunately, none of the above ideas has yet been put into practice by now.

4.7 Conclusion

Used as basic elements of sensitive IR detectors, lead telluride-based alloys doped with Group III atoms hold promise for the fabrication of advanced devices. The materials reviewed here have a number of unique properties, such as the internal integration of incident light flux, the fast and effective quenching of the built-up signal, high quantum efficiency (which is increased by a factor of up to 10^2 when using microwave pulses), the possibility of creating a 'continuous' IR image array and the availability of a read-out technique for its reading, and, finally, high radiation hardness.

The above properties of photodetectors on the basis of doped lead telluride alloys allow them to compete successfully with their most advanced analogues. The materials reviewed should be especially advantageous when operating in space-based systems, i.e., under weak-signal, low-background, hard-radiation conditions. Such conditions are realized, in particular, in space-based IR telescopes.

5. Summary

In this review, the whole body of data on impurity states in lead telluride-based compounds have been presented, which convincingly demonstrate that the behavior of some types of impurities is describable in terms of the mixed-valence model. The fact that quite a large number of dopants with widely different characteristics exhibit intermediate valences is indicative of important features of the crystal matrix. These features favor the formation of deep impurity states with an intermediate valence. However, the properties of such impurity states cannot be described in terms of simplified models that take into account only the features of the crystal matrix and neglecting the identity of the dopant.

Perhaps the clearest confirmation of this fact is that the valence changes by two on doping lead telluride with indium or gallium and by unity on doping it with chromium and ytterbium. Therefore, it does not yet seem possible, for all the systems considered here, to change from a phenomenological description relying on the locality or quasi-locality idea to microscopic models. This is due in large part to the experimental difficulties one faces in obtaining direct data on the structure of impurity energy spectra. Many conclusions concerning the behavior of the Group III impurities are based on indirect data and have been obtained from the analysis of available results — an approach which in principle cannot rule out ambiguity in interpretation.

Correlation effects in impurity – crystal lattice subsystems (which are manifested themselves, in particular, in the superposition of positive and negative photoconduction in PbTe(Ga) and in self-induced oscillations in In-doped solid solutions) and indeed the Fermi level stabilization effect itself, all reflect an interplay of a wide variety of factors, including the basic characteristics of the crystal matrix and impurity dopant as well as external influences. It turns out that while in this situation the characteristics of the quasi-stationary state in the presence of external influences play a key role, of no less importance is precisely which state is realized. This to a large extent complicates the description of nonequilibrium processes in an analytic way — which, however, is characteristic of virtually all multiparametric problems.

The discussion given in this paper clearly demonstrates the unique nature of the reviewed materials. The already existing information on impurity states in lead telluride and its solid solutions has provided significant insights into the behavior of impurities in semiconductors. Hopefully, further experimental and theoretical work will contribute importantly to the understanding of the fundamental aspects of the impurity problem as a whole.

Of particular interest are the applied aspects of the problem. Since the late 1970s, the prevailing view has been that, due to their low structural perfection, IV – VI semiconductors are noncompetitive as IR-optoelectronics materials. However, as further studies have shown, this view ignores the unique properties of impurity states in these materials. The latest results indicate that, as the basic element for highly sensitive far-infrared detectors, doped IV – VI semiconductors can compete successfully with the best world-respected analogues, and are therefore a very promising line of research.

Acknowledgements. The authors are grateful to B A Akimov, the author of many experimental studies and fruitful ideas that to a large extent determined the subject matter of this review.

This work has been supported in part by the Russian Foundation for Basic Research (Grants 01-02-16356, 02-02-17057, 00-15-96784), and INTAS (Grant 2001-0184).

References

1. Parada N J, Pratt G W (Jr) *Phys. Rev. Lett.* **22** 180 (1969)
2. Parada N J *Phys. Rev. B* **3** 2042 (1971)
3. Hemstreet L A *Phys. Rev. B* **11** 2260 (1975) **12** 1212 (1975)
4. Volkov B A, Pankratov O A *Dokl. Akad. Nauk SSSR* **255** 93 (1980) [*Sov. Phys. Dokl.* **25** 922 (1980)]
5. Bauer G et al. *J. Appl. Phys.* **47** 1721 (1976)
6. Hjalmarson H P et al. *Phys. Rev. Lett.* **44** 810 (1980)

7. Kaĭdanov V I, Ravich Yu I *Usp. Fiz. Nauk* **145** 51 (1985) [*Sov. Phys. Usp.* **28** 31 (1985)]
8. Kaĭdanov V I, Nemov S A, Ravich Yu I *Fiz. Tekh. Poluprovodn.* **28** 369 (1994) [*Semicond.* **28** 223 (1994)]
9. Nemov S A, Ravich Yu I *Usp. Fiz. Nauk* **168** 817 (1998) [*Phys. Usp.* **41** 735 (1998)]
10. Nimtz G, Schlicht B, in *Narrow Gap Semiconductors* (Springer Tracts in Modern Physics, Vol. 98, Ed. G Hohler) (Berlin: Springer-Verlag, 1983) p. 1
11. Lischka K *Phys. Status Solidi B* **133** 17 (1986)
12. Akimov B A et al. *Phys. Status Solidi A* **137** 9 (1993)
13. Partin D L *J. Appl. Phys.* **57** 1997 (1985)
14. Akimov B A et al. *Fiz. Tekh. Poluprovodn.* **25** 342 (1991) [*Semicond.* **25** 208 (1991)]
15. Vulchev V D, Borisova L D, Dimitrova S K *Phys. Status Solidi A* **97** K79 (1986)
16. Akimov B A et al. *Fiz. Tekh. Poluprovodn.* **23** 244 (1989) [*Sov. Phys. Semicond.* **23** 151 (1989)]
17. Akimov B A, Lvova N A, Ryabova L I *Phys. Rev. B* **58** 10430 (1998)
18. Story T et al. *Acta Phys. Pol. A* **84** 773 (1993)
19. Grodzicka E et al. *J. Cryst. Growth* **138** 1034 (1994)
20. Story T et al. *Acta Phys. Pol. A* **87** 229 (1995)
21. Grodzicka E et al. *Cryst. Res. Technol. S* **31** 651 (1996)
22. Vinogradova M N et al. *Fiz. Tekh. Poluprovodn.* **12** 663 (1978)
23. Bytenskiĭ L I et al. *Fiz. Tekh. Poluprovodn.* **18** 489 (1984) [*Sov. Phys. Semicond.* **18** 303 (1984)]
24. Novoselova A V et al. *Vestn. Mosk. Univ. Ser. 2. Khim.* **23** 3 (1982)
25. Moellmann K-P, Sishe D, Zajnudinov S *Crystal Res. Technol.* **21** 1273 (1986)
26. Lakeenkov V M et al. *Ukr. Fiz. Zh.* **29** 757 (1984)
27. Bushmarina G S et al. *Izv. Akad. Nauk SSSR, Neorg. Mater.* **23** 222 (1987)
28. Veĭs A N et al. *Fiz. Tekh. Poluprovodn.* **7** 928 (1973)
29. Akimov B A et al. *Fiz. Tekh. Poluprovodn.* **17** 87 (1983) [*Sov. Phys. Semicond.* **17** 53 (1983)]
30. Sizov F F, Plyatsko S V, Lakeenkov V M *Fiz. Tekh. Poluprovodn.* **19** 592 (1985)
31. Belokon' S A et al. *Fiz. Tekh. Poluprovodn.* **26** 264 (1992) [*Semicond.* **26** 148 (1992)]
32. Skipetrov E P et al., in *Material Science and Material Properties for Infrared Optoelectronics* (Proc. SPIE, Vol. 3182, Eds F F Sizov, V V Tetyorkin) (Bellingham, WA: SPIE, 1997) p. 228
33. Brandt N B, Skipetrov E P *Fiz. Nizk. Temp.* **22** 870 (1996) [*Low-Temp. Phys.* **22** 665 (1996)]
34. Dolzhenko D E et al. *Fiz. Tekh. Poluprovodn.* **34** 1194 (2000) [*Semicond.* **34** 1144 (2000)]
35. Akimov B A et al. *Fiz. Tekh. Poluprovodn.* **17** 1604 (1983)
36. Kashirskaya L M et al. *Fiz. Tekh. Poluprovodn.* **24** 1349 (1990) [*Sov. Phys. Semicond.* **24** 848 (1990)]
37. Kaĭdanov V I, Mel'nik R B, Chernik I A *Fiz. Tekh. Poluprovodn.* **7** 759 (1973)
38. Kaĭdanov V I, Nemov S A, Ravich Yu I *Fiz. Tekh. Poluprovodn.* **26** 201 (1992) [*Semicond.* **26** 113 (1992)]
39. Chernik I A, Lykov S N *Pis'ma Zh. Tekh. Fiz.* **7** 94 (1981) [*Sov. Tech. Phys. Lett.* **7** 40 (1981)]
40. Kaĭdanov V I et al. *Pis'ma Zh. Eksp. Teor. Fiz.* **35** 517 (1982) [*JETP Lett.* **35** 639 (1982)]
41. Nemov S A, Bogatyrenko N G, Proshin V I *Fiz. Tekh. Poluprovodn.* **24** 1391 (1990) [*Sov. Phys. Semicond.* **24** 873 (1990)]
42. Kaĭdanov V I, Rykov S A, Rykova M A *Fiz. Tverd. Tela* **31** (8) 68 (1989) [*Sov. Phys. Solid State* **31** 1316 (1989)]
43. Veĭs A N et al. *Fiz. Tekh. Poluprovodn.* **11** 995 (1977) [*Sov. Phys. Semicond.* **11** 588 (1977)]
44. Kaĭdanov V I, Mel'nik R B, Nemov S A *Fiz. Tekh. Poluprovodn.* **13** 1011 (1979) [*Sov. Phys. Semicond.* **13** 591 (1979)]
45. Prokof'eva L V, Vinogradova M N, Zarubo S V *Fiz. Tekh. Poluprovodn.* **14** 2201 (1980)
46. Prokof'eva L V et al. *Pis'ma Zh. Eksp. Teor. Fiz.* **33** 14 (1981) [*JETP Lett.* **33** 12 (1981)]
47. Vulchev V D, Borisova L D *Phys. Status Solidi A* **99** K53 (1987)
48. Ivanchik I I et al., in *Proc. of the 24th Intern Conf. on the Physics of Semiconductors, Aug. 2–7, 1998, Jerusalem, Israel* Vol. 2 (Ed. G Gershoni) (Singapore: World Scientific, 1999) p. Th1 – D3
49. Akimov B A et al. *Fiz. Tekh. Poluprovodn.* **13** 752 (1979) [*Sov. Phys. Semicond.* **13** 441 (1979)]
50. Takaoka S, Itoga T, Murase K *Jpn. J. Appl. Phys.* **23** 216 (1984)
51. Akimov B A et al. *Fiz. Tekh. Poluprovodn.* **23** 1019 (1989) [*Sov. Phys. Semicond.* **23** 636 (1989)]
52. Lebedev A I, Abdullin Kh A *Fiz. Tekh. Poluprovodn.* **18** 624 (1984)
53. Bocharova T V et al. *Fiz. Tekh. Poluprovodn.* **16** 1462 (1982)
54. Akimov B A et al. *Fiz. Tekh. Poluprovodn.* **25** 250 (1991) [*Semicond.* **25** 152 (1991)]
55. Akimov B A et al. *Fiz. Tekh. Poluprovodn.* **27** 351 (1993) [*Semicond.* **27** 194 (1993)]
56. Grodzicka E et al. *Acta Phys. Pol. A* **90** 801 (1996)
57. Vygranenko Yu K, Slyn'ko V E, Slyn'ko E I *Neorg. Mater.* **31** 1338 (1995) [*Inorg. Mater.* **31** 1219 (1995)]
58. Mahoukou F et al. *Phys. Status Solidi B* **195** 511 (1996)
59. Story T *Acta Phys. Pol. A* **92** 663 (1997)
60. Skipetrov E P et al. *Phys. Status Solidi B* **210** 289 (1998)
61. Skipetrov E P et al. *Phys. Rev. B* **59** 12928 (1999)
62. Story T et al. *Acta Phys. Pol. A* **92** 997 (1997)
63. Story T et al. *Acta Phys. Pol. A* **82** 879 (1992)
64. Akimov B A et al. *Fiz. Tekh. Poluprovodn.* **13** 1293 (1979)
65. Akimov B A et al. *Pis'ma Zh. Eksp. Teor. Fiz.* **31** 304 (1980) [*JETP Lett.* **31** 279 (1980)]
66. Skipetrov E P et al. *J. Cryst. Growth* **210** 292 (2000)
67. Akimov B A et al. *Pis'ma Zh. Eksp. Teor. Fiz.* **29** 11 (1979) [*JETP Lett.* **29** 9 (1979)]
68. Akimov B A et al. *J. Low Temp. Phys.* **51** 9 (1983)
69. Akimov B A, Ryabova L I, Chudinov S M *Fiz. Tverd. Tela* **21** 708 (1979)
70. Tsidil'kovskiĭ I M, Kuleev I G, Lyapilin I I *Zh. Eksp. Teor. Fiz.* **102** 326, 1652 (1992) [*Sov. Phys. JETP* **75** 172, 893 (1992)]; Mycielski J *Solid State Commun.* **60** 165 (1986)
71. Ivanchik I I et al. *Phys. Rev. B* **61** R14889 (2000)
72. Skipetrov E P et al. *Izv. Vyssh. Ucheb. Zaved. Mater. Élektr. Tekh.* **1** (3) 68 (1998)
73. Sheĭkman M K, Shik A Ya *Fiz. Tekh. Poluprovodn.* **10** 208 (1976) [*Sov. Phys. Semicond.* **10** 128 (1976)]
74. Lo I et al. *Appl. Phys. Lett.* **60** 751 (1992)
75. Mooney P M *J. Appl. Phys.* **67** (3) R1 (1990); Chadi D J, Chang K J *Phys. Rev. Lett.* **61** 873 (1988)
76. Vul B M *Pis'ma Zh. Eksp. Teor. Fiz.* **29** 21 (1979) [*JETP Lett.* **29** 18 (1979)]
77. Akimov B A et al. *Phys. Lett. A* **88** 483 (1982)
78. Akimov B A et al. *Vysokochistye Veshchestva* (6) 22 (1991)
79. Volkov B A, Voronova I D, Shotov A P *Dokl. Akad. Nauk SSSR* **293** 602 (1987)
80. Vul B M *Pis'ma Zh. Eksp. Teor. Fiz.* **33** 346 (1981) [*JETP Lett.* **33** 329 (1981)]
81. Martinez A et al. *J. Appl. Phys.* **57** 1165 (1985)
82. Martinez A et al. *J. Appl. Phys.* **58** 4618 (1985)
83. Moellmann K-P, Herrmann K H, Enderlein R, in *Proc. of the 16th Intern. Conf. on the Physics of Semiconductors, Montpellier, 1982*; *Physica B* **117/118** 582 (1983)
84. Herrmann K H, Moellmann K-P, Wendt M *Phys. Status Solidi A* **80** 541 (1983)
85. Lebedev A I, Aĭtikeeva T D *Fiz. Tekh. Poluprovodn.* **18** 1964 (1984)
86. Troyan Yu G, Sizov F F, Lakeenkov V M *Fiz. Tekh. Poluprovodn.* **20** 1776 (1986)
87. Akimov B A et al. *Semicond. Sci. Technol.* **14** 679 (1999)
88. Akimov B A et al. *Fiz. Tekh. Poluprovodn.* **35** 524 (2001) [*Semicond.* **35** 502 (2001)]
89. Akimov B A et al. *Phys. Rev. B* **61** 16045 (2000)
90. Akimov B A et al. *Pis'ma Zh. Eksp. Teor. Fiz.* **39** 222 (1984) [*JETP Lett.* **39** 265 (1984)]
91. Akimov B A, Albul A V, Ryabova L I *Fiz. Tekh. Poluprovodn.* **29** 2158 (1995) [*Semicond.* **29** 1125 (1995)]
92. Zasavitskiĭ I I et al. *Fiz. Tekh. Poluprovodn.* **21** 1789 (1987)
93. Zasavitskiĭ I I, Matsonashvili B N, Trofimov V T *Fiz. Tekh. Poluprovodn.* **23** 2019 (1989) [*Sov. Phys. Semicond.* **23** 1249 (1989)]
94. Zasavitskiĭ I I et al. *Pis'ma Zh. Eksp. Teor. Fiz.* **42** 3 (1985) [*JETP Lett.* **42** 1 (1985)]
95. Zasavitskiĭ I I et al. *Fiz. Tekh. Poluprovodn.* **20** 214 (1986)
96. Krotkus A et al. *Solid State Electron.* **26** 605 (1983)

97. St-Onge H, Walpole J N *Phys. Rev. B* **6** 2337 (1972)
98. Krotkus A, Plitnikas P, Shimkene U *Fiz. Tekh. Poluprovodn.* **17** 2180 (1983)
99. Jantsch W, Rozenbergs J, Heinrich H *Solid State Electron.* **21** 103 (1972)
100. Jantsch W, Rozenbergs J, Heinrich H *Solid State Commun.* **17** 1145 (1975)
101. Krotkus A et al. *Lit. Fiz. Sbornik* **26** 582 (1986)
102. Akimov B A, Brandt N B, Nikiforov V N *Fiz. Tverd. Tela* **26** 1602 (1984)
103. Akimov B A et al. *Solid State Commun.* **43** 31 (1982)
104. Happ M, Moellmann K-P *Phys. Status Solidi A* **91** K159 (1985)
105. Herrmann K H et al. *Phys. Status Solidi A* **71** K21 (1982)
106. Herrmann K H, Moellmann K-P *Phys. Status Solidi A* **80** K101 (1983)
107. Akimov B A, Khokhlov D R, Chesnokov S N *Fiz. Tekh. Poluprovodn.* **23** 899 (1989)
108. Abramyan Yu A, Papazyan K Z, Stafeev V I *Fiz. Tekh. Poluprovodn.* **24** 1752 (1990) [*Sov. Phys. Semicond.* **24** 1093 (1990)]
109. Akimov B A, Albul A V, Bogdanov E V *Semicond. Sci. Technol.* **8** S447 (1993)
110. Akimov B A et al. *Fiz. Tekh. Poluprovodn.* **28** 232 (1994) [*Semicond.* **28** 140 (1994)]
111. Veĭs A N, Yafaev R R *Fiz. Tekh. Poluprovodn.* **18** 475 (1984)
112. Veĭs A N, Glebova E V *Izv. Vyssh. Ucheb. Zaved. Fiz.* **26** 117 (1983)
113. Drabkin I A et al. *Fiz. Tekh. Poluprovodn.* **7** 794 (1973)
114. Veĭs A N, Kaĭdanov V I, Nemov S A *Fiz. Tekh. Poluprovodn.* **12** 1599 (1978) [*Sov. Phys. Semicond.* **12** 943 (1978)]
115. Bocharova T V et al. *Fiz. Tekh. Poluprovodn.* **15** 175 (1981)
116. Veĭs A N et al. *Fiz. Tekh. Poluprovodn.* **10** 104 (1976)
117. Lideikis T et al. *Solid State Commun.* **57** 583 (1986)
118. Takaoka S, Murase K *J. Phys. Soc. Jpn* **52** 25 (1983)
119. McKnight S W, El-Rayess M K *Solid State Commun.* **49** 1001 (1984)
120. McKnight S W, El-Rayess M K *J. Phys. C* **17** 6893 (1984)
121. Takaoka S et al. *Solid State Commun.* **54** 99 (1985)
122. Ishigushi T, Drew H W, in *Proc. of the 17th Intern. Conf. on the Physics of Semiconductors, Aug., 1984, San-Francisco, USA*, Book of Abstracts (1984) p. 319
123. Akimov B A et al. *Zh. Eksp. Teor. Fiz.* **87** 1349 (1984) [*Sov. Phys. JETP* **60** 782 (1984)
124. Romcevic N et al. *Phys. Rev. B* **43** 6712 (1991)
125. Belogorokhov A I et al. *Fiz. Tverd. Tela* **34** 1651 (1992) [*Sov. Phys. Solid State* **34** 873 (1992)]
126. Romcevic N, Popovic Z V, Khokhlov D R *J. Phys: Condens. Mat.* **7** 5105 (1995)
127. Khokhlov D R, Volkov B A, in *Proc. of the 23rd Intern. Conf. on the Physics of Semiconductors, July 21 – 26, Berlin* Vol. 4 (Ed. M Schefler) (Singapore: World Scientific, 1996) p. 2941
128. Akimov B A et al. *Pis'ma Zh. Tekh. Fiz.* **6** 1269 (1980)
129. Abdullin Kh A, Lebedev A I *Fiz. Tekh. Poluprovodn.* **19** 1725 (1985)
130. Abdullin Kh A, Lebedev A I *Pis'ma Zh. Eksp. Teor. Fiz.* **39** 272 (1984) [*JETP Lett.* **39** 325 (1984)]
131. Herrmann K H, Moellmann K-P *Phys. Status Solidi A* **91** K147 (1985)
132. Moellmann K-P, Happ M *Phys. Status Solidi A* **91** K71 (1985)
133. McKnight S W, El-Rayess M K *Semicond. Sci. Technol.* **6** C42 (1991)
134. Chishko V F et al. *Infrared Phys.* **33** 197 (1992)
135. Bushmarina G S et al. *Fiz. Tekh. Poluprovodn.* **11** 1874 (1977)
136. Belogorokhov A I, Slyn'ko E I, Khokhlov D R *Pis'ma Zh. Tekh. Fiz.* **18** 30 (1992) [*Sov. Tech. Phys. Lett.* **18** 252 (1992)]
137. Grishechkina S P et al. *Fiz. Tekh. Poluprovodn.* **25** 677 (1991) [*Sov. Phys. Semicond.* **25** 409 (1991)]
138. Akimov B A et al. *Fiz. Tekh. Poluprovodn.* **29** 2015 (1995) [*Semicond.* **29** 1051 (1995)]
139. Belogorokhov A I et al. *Brasil. J. Phys.* **26** 308 (1996)
140. Volkov B A, Ruchaĭskiĭ O M *Pis'ma Zh. Eksp. Teor. Fiz.* **62** 205 (1995) [*JETP Lett.* **62** 217 (1995)]
141. Kaĭdanov V I et al. *Fiz. Tekh. Poluprovodn.* **24** 144 (1990) [*Sov. Phys. Semicond.* **24** 87 (1990)]
142. Vinchakov V N et al. *Pis'ma Zh. Eksp. Teor. Fiz.* **43** 384 (1986) [*JETP Lett.* **43** 495 (1986)]
143. Vinchakov V N, Kaĭdanov V I, Rykov S A *Fiz. Tekh. Poluprovodn.* **15** 2335 (1981)
144. Akimov B A, L'vova N A, Ryabova L I *Fiz. Tekh. Poluprovodn.* **30** 1647 (1996) [*Semicond.* **30** 861 (1996)]
145. Drabkin I A, Kvantov M A, Kompaneets V V *Fiz. Tekh. Poluprovodn.* **13** 2064 (1979)
146. Mac W, Story T, Twardowski A *Acta Phys. Pol. A* **87** 492 (1995)
147. Vasil'ev A N et al. *Zh. Eksp. Teor. Fiz.* **114** 1859 (1998) [*JETP* **87** 1009 (1998)]
148. Akimov B A et al., in *Infrared Applications of Semiconductors II: Symp., Dec. 4, 1997, Boston, Mass., USA* (Materials Research Society Symp. Proc., Vol. 484, Eds D L McDaniel et al.) (Pittsburgh, PA: Materials Research Soc., 1998) p. 359
149. Akimov B A et al. *Phys. Status Solidi B* **210** 787 (1998)
150. Akimov B A et al. *Fiz. Tekh. Poluprovodn.* **31** 133 (1997) [*Semicond.* **31** 100 (1997)]
151. Akimov B A et al. *Fiz. Tekh. Poluprovodn.* **23** 668 (1989) [*Sov. Phys. Semicond.* **23** 418 (1989)]
152. Khokhlov D R et al. *Physica B* **177** 491 (1992)
153. de Visser A et al. *Fiz. Tekh. Poluprovodn.* **26** 1034 (1992) [*Sov. Phys. Semicond.* **26** 579 (1992)]
154. Khokhlov D R et al. *Solid State Commun.* **82** 759 (1992)
155. Kagan Yu M, Kikoin K A *Pis'ma Zh. Eksp. Teor. Fiz.* **31** 367 (1980) [*JETP Lett.* **31** 335 (1980)]
156. Litvinov V I, Tovstyuk K D *Fiz. Tverd. Tela* **24** 896 (1982)
157. Pankratov O A, Volkov B A *Zh. Eksp. Teor. Fiz.* **88** 280 (1985) [*Sov. Phys. JETP* **61** 164 (1985)]
158. Pankratov O A, Volkov B A *Sov. Sci. Reviews Sect. A Phys. Rev.* (Ed. I M Khalatnikov) **9** 355 (1987)
159. Pankratov O A, Povarov P P *Solid State Commun.* **66** 847 (1988)
160. Drabkin I A, Moĭzhes B Ya *Fiz. Tekh. Poluprovodn.* **15** 625 (1981) [*Sov. Phys. Semicond.* **15** 357 (1981)]
161. Belogorokhov A I et al. *Pis'ma Zh. Eksp. Teor. Fiz.* **72** 178 (2000) [*JETP Lett.* **72** 123 (2000)]
162. Baz' A I, Zel'dovich Ya B, Perelomov A M *Rasseyanie, Reaktsii i Raspady v Nerelyativistkoĭ Kvantovoĭ Mekhanike* 2nd ed. (Scattering, Reactions and Decays in Non-Relativistic Quantum Mechanics) (Moscow: Nauka, 1971) Ch. 1, Sections 3, 4
163. Bethe H A *Intermediate Quantum Mechanics* (New York: W.A. Benjamin, 1964) [Translated into Russian (Moscow: Mir 1965) p. 191]
164. Wolf J, Lemke D *Infrared Phys.* **25** 327 (1985)
165. Haller E E, Hueschen M R, Richards P L *Appl. Phys. Lett.* **34** 495 (1979)
166. Reynolds D B et al. *IEEE Trans. Nucl. Sci.* **NS-36** 857 (1989)
167. Wu I C et al. *Appl. Phys. Lett.* **58** 1431 (1991)
168. Lambrecht A et al. *Semicond. Sci. Technol.* **8** S334 (1993)
169. Zogg H et al. *Semicond. Sci. Technol.* **6** C36 (1991)
170. Skipetrov E P, Nekrasova A N, Khorosh A G *Fiz. Tekh. Poluprovodn.* **28** 815 (1994) [*Semicond.* **28** 478 (1994)]
171. Akimov B A, Private communication
172. Akimov B A et al. *Infrared Phys.* **34** 375 (1993)
173. Akimov B A et al. *Pis'ma Zh. Tekh. Fiz.* **14** 731 (1988)
174. Akimov B A, Khokhlov D R *Semicond. Sci. Technol.* **8** S349 (1993)
175. Dolzhenko D E et al. *Pis'ma Zh. Eksp. Teor. Fiz.* **55** 125 (1992) [*JETP Lett.* **55** 119 (1992)]
176. Golubev V G et al. *Fiz. Tekh. Poluprovodn.* **11** 1704 (1977)
177. Khokhlov D R et al. *Appl. Phys. Lett.* **76** 2835 (2000)
178. Belogorokhov A I et al. *Pis'ma Zh. Eksp. Teor. Fiz.* **63** 342 (1996) [*JETP Lett.* **63** 353 (1996)]
179. Chesnokov S N et al. *Infrared Phys.* **35** 23 (1994)
180. Akimov B A et al. *Solid State Commun.* **66** 811 (1988)